

# QuantKAN: A Unified Quantization Framework for Kolmogorov–Arnold Networks

Kazi Ahmed Asif Fuad<sup>1</sup> Lizhong Chen<sup>1</sup>

## Abstract

Kolmogorov–Arnold Networks (KANs) replace linear weights with spline-based functions, offering strong expressivity but posing challenges for low-precision deployment due to heterogeneous parameter distributions. We introduce QuantKAN, the first unified framework for quantization-aware training (QAT) and post-training quantization (PTQ) of KANs. The framework employs branch-aware quantizers for base and spline parameters and extends modern QAT and PTQ methods to spline-based layers across EfficientKAN, FastKAN, PyKAN, and KAGN. Experiments on MNIST, CIFAR-10/100, Tiny-ImageNet, and ImageNet provide the first low-precision KAN benchmarks and show that DSQ is the most robust QAT method at aggressive low-bit settings, while GPTQ is the strongest PTQ method at moderate precision. Parameter-wise sensitivity analyses reveal that spline/basis components are often the dominant failure mode, motivating mixed-precision designs that allocate bits where they matter most. QuantKAN is available at <https://github.com/OSU-STARLAB/QuantKAN/>.

## 1. Introduction

Neural networks built on spline-based function approximators, such as Kolmogorov–Arnold Networks (KANs) (Liu et al., 2025), have recently emerged as interpretable and efficient alternatives to multilayer perceptrons (MLPs) and convolutional networks (CNNs). Variants including EfficientKAN (Blealtan & Dash, 2024), FastKAN (Li, 2024), PyKAN (Liu et al., 2025), and KAGN (Drokin, 2024; Khochawongwat, 2024) demonstrate that spline expansions can replace or augment linear transformations, providing

<sup>1</sup>Department of EECS, Oregon State University, Oregon, USA. Correspondence to: Kazi Ahmed Asif Fuad <fuadk@oregonstate.edu>, Lizhong Chen <chen-liz@oregonstate.edu>.

Preprint. January 30, 2026.

flexible inductive biases with strong empirical performance. However, the expressive basis functions that give KANs their representational power also complicate use in resource-constrained settings.

Quantization is a central technique for efficient model deployment, enabling reduced-precision inference in both convolutional neural networks and Transformer architectures (Jacob et al., 2017; Nagel et al., 2020; Li et al., 2021; Dong et al., 2019a; Frantar et al., 2023; Lin et al., 2024; Xiao et al., 2024). Yet, there is no systematic exploration of quantization for spline-based architectures. Existing quantization methods often assume Gaussian-like weight distributions or convolution-friendly structures, which fail to generalize to the heterogeneous, branch-specific distributions of spline expansions or polynomial convolutions. Moreover, the lack of KAN-specific tooling makes quantization design and debugging time-consuming, hindering efficient adoption.

To address this gap, we introduce **QuantKAN**, the first unified framework for quantizing KANs. QuantKAN supports both quantization-aware training (QAT) (Esser et al., 2020; Gong et al., 2019) and post-training quantization (PTQ) (Nagel et al., 2020; Frantar et al., 2023), extending these methods to spline-based layers, including base, spline, and polynomial branches. The modular design enables integration of classic and modern quantizers while accounting for the unique distributions and sensitivities of KAN parameters. We conduct extensive experiments across MNIST, CIFAR-10/100, TinyImageNet, and ImageNet, and across multiple KAN variants, complemented by systematic ablations that reveal distinct quantization behaviors in spline networks.

This work establishes systematic baselines and design guidelines for low-precision KANs, offering practical tooling and empirical insights into their quantization behavior. QuantKAN bridges spline-based representations with modern quantization techniques, clarifying how architectural structure and parameter heterogeneity influence reduced-precision KAN inference. Our main contributions are summarized as follows:

- *QuantKAN Framework:* We introduce QuantKAN, a unified framework supporting both quantization-aware training (QAT) and post-training quantization (PTQ)

for KANs, extending representative QAT and PTQ methods to spline- and polynomial-based layers in an implementation-aligned manner.

- *Branch-Aware Quantization for KANs:* We develop modular, branch-aware quantization wrappers for EfficientKAN, FastKAN, PyKAN, and KAGN, enabling independent quantization of base weights, spline/basis parameters, and activations to account for heterogeneous statistics and sensitivities.
- *Comprehensive Evaluation and Design Insights:* We establish benchmarks for quantized KANs on MNIST, CIFAR-10/100, TinyImageNet, and ImageNet, complemented by extensive ablations that reveal method–architecture interactions, parameter-wise sensitivity, and mixed-precision design principles for robust low-bit KAN inference.

## 2. Background and Related Work

### 2.1. Quantization in Neural Networks

Quantization has long been a cornerstone for efficient deployment of neural networks, reducing both memory and compute costs by mapping floating-point values to lower-precision integer domains (Gholami et al., 2021). Broadly, methods are categorized into *quantization-aware training* (QAT) and *post-training quantization* (PTQ).

QAT inserts “fake-quantization” operations during training so that the model learns to adapt to quantization noise. Classical approaches include DoReFa (Zhou et al., 2018), PACT (Choi et al., 2018), QIL (Jung et al., 2018), LSQ (Esser et al., 2020), LSQ+ (Bhalgat et al., 2020), and DSQ (Gong et al., 2019). These methods learn clipping thresholds, step sizes, or soft relaxations, but assume relatively homogeneous weight distributions (e.g., Gaussian-like) typical of CNN and Transformer layers.

PTQ instead compresses pretrained models with little or no retraining, often relying on small calibration datasets. Representative methods include AdaRound (Nagel et al., 2020), BRECCQ (Li et al., 2021), and GPTQ (Frantar et al., 2023), which optimize rounding or reconstruction at the block or layer level. Hessian-aware bit allocation methods such as HAWQ and HAWQ-V2 (Dong et al., 2019b;a) leverage curvature information to guide mixed-precision assignment. Recent methods also address activation outliers, e.g., AWQ (Lin et al., 2024) and SmoothQuant (Xiao et al., 2024), while data-free PTQ is enabled by ZeroQ (Cai et al., 2020). Together, these advances demonstrate the maturity of quantization research for standard architectures, but none directly address spline-based networks.

### 2.2. Kolmogorov–Arnold Networks (KANs)

Kolmogorov–Arnold Networks (KANs) are inspired by the Kolmogorov–Arnold representation theorem, which states that any multivariate function can be decomposed into a composition of univariate functions and summations. Unlike MLPs, where weights are linear scalars, KANs replace each weight with a learnable spline function, placing nonlinearities on edges rather than nodes. This leads to strong approximation power, favorable scaling laws, and enhanced interpretability, as each edge encodes an adaptive basis function (Liu et al., 2025).

Variants proliferated. EfficientKAN introduces stable spline bases and efficient evaluation strategies (Blealtan & Dash, 2024); FastKAN replaces splines with radial basis functions to accelerate computation (Li, 2024); PyKAN provides a general-purpose implementation for scientific applications (Liu et al., 2025); and convolutional variants such as KAGN extend KANs with GRAM-based bases for structured data (Drokin, 2024; Khochawongwat, 2024). While KANs offer promising accuracy–efficiency tradeoffs, recent analyses caution that their benefits are domain-specific compared to matched MLPs (Yu et al., 2024).

This dual branch structure, consisting of linear base weights and nonlinear spline coefficients, is central to both the expressivity and the quantization challenges of KANs. These parameter groups exhibit distinct statistical properties, including different variance profiles and tail behaviors, which complicates the direct application of existing quantization schemes. Despite rapid progress in neural network quantization and the proliferation of KAN variants, no prior work has systematically studied quantization for spline based architectures. Most existing methods assume relatively homogeneous weight distributions or standardized activation placement, assumptions that are violated by the branch structure and spline expansions in KANs. As a result, directly applying quantizers developed for CNNs or Transformers often leads to instability or significant accuracy degradation.

Our work fills this gap with **QuantKAN**, the first unified framework for quantizing KANs. It extends QAT and PTQ to explicitly handle base and spline branches, systematically evaluates multiple KAN variants across datasets, and establishes the first baselines for low-bit KAN deployment.

## 3. The QuantKAN Framework

QuantKAN is a unified framework for quantizing KANs under low-bit precision. Quantizing KANs is fundamentally different from conventional architectures like CNNs because each KAN layer decomposes into two functionally distinct pathways: a *base branch* that applies learned linear weights to a simple nonlinearity, and a *spline/basis branch* that computes a flexible basis expansion (e.g., B-splines, RBFs, or

Gram polynomials) followed by learned coefficients. These branches serve different roles and exhibit distinct statistics and sensitivities during training.

We empirically observe in Figure 1 that pronounced distributional heterogeneity across KAN branches: base weights often exhibit heavier tails and outliers, while spline/basis parameters are frequently more concentrated, though this pattern can vary by architecture (see Appendix A). Importantly, distributional width alone does *not* reliably predict quantization sensitivity; our sensitivity and ablation results (Section 5.4) show that spline/basis parameters can be disproportionately sensitive to quantization error despite appearing well-behaved. This combination makes naive “single-quantizer” strategies unreliable.

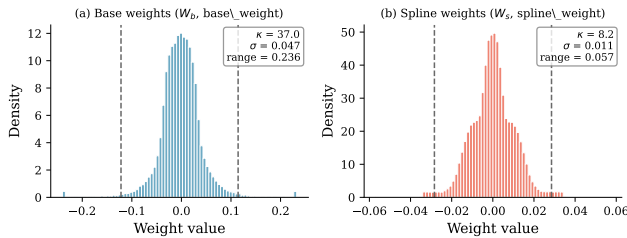


Figure 1. Branch-wise weight distributions in a trained KAN. Base weights exhibit heavier tails and a wider dynamic range ( $\approx 0.236$ ) than spline/basis weights ( $\approx 0.057$ ), a scale difference of about  $4.1\times$ . Dashed lines indicate the 1st and 99th percentiles.

**Branch-aware quantization.** QuantKAN addresses this by maintaining *independent quantizers* for (i) base weights, (ii) spline/basis weights, and (iii) activations. Let  $x$  denote the layer input,  $W_b$  the base weights,  $W_s$  the spline/basis coefficients,  $\sigma(\cdot)$  the base activation (e.g., SiLU), and  $\Phi(x)$  the basis expansion. A full-precision KAN layer computes

$$y = f(x) = \underbrace{W_b \cdot \sigma(x)}_{\text{base branch}} + \underbrace{W_s \cdot \Phi(x)}_{\text{spline/basis branch}}. \quad (1)$$

Under quantization, we apply separate quantizers to each component:

$$\hat{y} = f_q(x) = Q_b(W_b) \sigma(Q_a(x)) + Q_s(W_s) \Phi(Q_a(x)), \quad (2)$$

where each quantizer  $Q(\cdot; \theta)$  is parameterized by learnable and/or calibrated parameters  $\theta$  (e.g., step size, clipping bounds, optional zero-point), optimized *independently* per branch. In our experiments, collapsing branches into a shared quantizer often destabilizes scaling and significantly degrades accuracy, whereas branch-aware quantization consistently improves robustness at low bit-widths.

**Unified coverage across KAN variants.** QuantKAN provides architecture-aware wrappers (e.g., QuantKANLinear, QuantFastKANLayer, QuantPyKANLayer, QuantGRAMLayer, and

QuantKAGNConv) that implement branch-aware quantization consistently across KAN variants. The framework supports two complementary modes: (i) **quantization-aware training (QAT)**, where quantizers are integrated during training and optimized jointly with the model; and (ii) **post-training quantization (PTQ)**, where pretrained models are quantized post hoc using calibration and/or reconstruction objectives.

### 3.1. Quantization-Aware Training for KANs

QAT integrates quantizers into the forward pass while approximating gradients through the discrete operations using a straight-through estimator (STE). For KANs, this setup is more delicate than in CNNs/Transformers due to the dual-branch structure and heterogeneous statistics. QuantKAN therefore quantizes three components separately: base weights, spline/basis weights, and activations. Concretely, the quantized forward pass follows Eq. (2). Figure 2 illustrates the QAT dataflow where both branches are quantized independently and their outputs are summed.

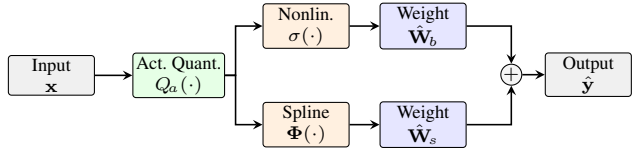


Figure 2. Quantization-aware training dataflow for a KAN layer. Input activations are quantized via  $Q_a$ , then processed through parallel base ( $\sigma \rightarrow \hat{W}_b$ ) and spline ( $\Phi \rightarrow \hat{W}_s$ ) branches. Independent quantizers enable mixed-precision allocation across branches.

We evaluate and compare QAT methods that represent complementary design axes that are especially relevant for KANs: (i) *step-size learning* (LSQ/LSQ+) to adapt quantization scales to heterogeneous branch distributions; (ii) *learned clipping and interval shaping* (PACT, QIL) to control outliers and enforce effective dynamic ranges; (iii) *non-adaptive baselines* (DoReFa) to quantify the benefit of learning quantizer parameters; and (iv) *smooth relaxation of rounding* (DSQ) to improve optimization stability when spline/basis pathways are quantized aggressively. All methods use branch-aware quantization with independent base and spline parameters, as shared quantizers often mismatch KAN statistics and destabilize low-precision training.

### 3.2. Post-Training Quantization (PTQ) for KANs

PTQ compresses pretrained models without retraining, using small calibration sets or data-free synthesis. For KANs, PTQ is challenging because base and spline parameters exhibit different dynamic ranges and curvature, causing branch-specific error accumulation. QuantKAN therefore calibrates or reconstructs base and spline branches sepa-

rately. Let  $Q(\cdot)$  denote a branch-wise quantizer parameterized by scale(s) and optional zero-point(s).

$$\hat{W}_b = Q(W_b; \alpha_b, z_b), \quad \hat{W}_s = Q(W_s; \alpha_s, z_s), \quad (3)$$

and optimize them with a branch-aware reconstruction objective:

$$\begin{aligned} \mathcal{L}_{\text{PTQ}} = & \lambda_b \|f_b(x; \hat{W}_b) - f_b(x; W_b)\|_2^2 \\ & + \lambda_s \|f_s(x; \hat{W}_s) - f_s(x; W_s)\|_2^2 \\ & + \|f(x; \hat{W}_b, \hat{W}_s) - f(x; W_b, W_s)\|_2^2, \end{aligned} \quad (4)$$

where  $f_b$  and  $f_s$  denote the base and spline/basis branches and  $f$  is the full layer mapping. Different PTQ methods (e.g., AdaRound, BRECQ, GPTQ, AWQ, SmoothQuant, HAWQ-V2, ZeroQ) instantiate this objective with different calibration and optimization strategies; QuantKAN adapts each method by preserving branch separation throughout calibration/reconstruction.

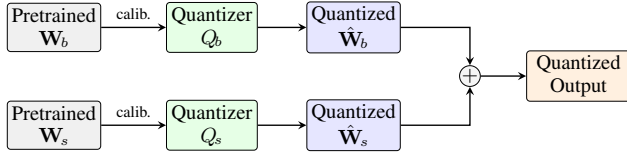


Figure 3. Post-training quantization (PTQ) for a KAN layer. Base and spline weights are independently quantized via calibration-based quantizers  $Q_b$  and  $Q_s$ , then combined to produce the final quantized output.

We evaluate PTQ methods that span the major families used in modern low-bit deployment while exposing how they interact with KAN-specific branch heterogeneity. Uniform and percentile calibration provide necessary baselines for scale selection under heavy-tailed weights. AdaRound and BRECQ represent *reconstruction-based* PTQ that directly minimizes functional error, which is critical when spline/basis parameters are sensitive to small perturbations. AWQ and SmoothQuant represent *outlier- and activation-aware* scaling, which is relevant because KAN activations and basis expansions can produce imbalanced magnitudes across channels. GPTQ provides a *second-order* approximation that is effective at very low precision by compensating quantization error using curvature information; in QuantKAN, we estimate these statistics separately for base and spline/basis weights. Finally, ZeroQ enables a *data-free* operating point when calibration data is limited, serving as a practical fallback in deployment settings. All PTQ methods are applied in a branch-aware manner to preserve KAN layer structure and avoid scale coupling between pathways.

## 4. Experimental Setup

**Models and datasets.** We evaluate QuantKAN on multiple Kolmogorov–Arnold Network (KAN) variants, in-

cluding PyKAN, EfficientKAN, FastKAN, GRAM-KAN, and KAGN-style convolutional KANs, spanning both fully connected and convolutional settings. Experiments are conducted on standard image classification benchmarks: MNIST, CIFAR-10/100, TinyImageNet, and ImageNet.

**Training and evaluation.** All models are first trained in full precision. Quantization-aware training (QAT) initializes from pretrained checkpoints and inserts quantizers into the forward pass (Section 3); QAT models are fine-tuned for 5–20 epochs depending on dataset size. Post-training quantization (PTQ) operates on the same checkpoints using calibration or reconstruction without task retraining. We report Top-1 accuracy on the test set unless stated otherwise.

**Quantization configuration.** We study weight-only and joint weight–activation quantization at 2–8 bits using the branch-aware design of QuantKAN, with independent quantizers for base weights, spline/basis weights, and activations. We denote configurations as  $w_x$  for weight-only quantization with full-precision activations ( $a=32$ ), and  $w_x a_y$  for joint quantization, where  $x$  and  $y$  indicate the bit-widths of weights and activations. We evaluate per-tensor and per-channel scaling, as well as symmetric and asymmetric quantization, via controlled ablations.

For QAT, we evaluate representative step-size, clipping-based, smooth-relaxation, and baseline methods (LSQ/LSQ+, PACT, QIL, DSQ, DoReFa). For PTQ, we compare calibration-based, reconstruction-based, activation-aware, second-order, and data-free approaches (Uniform, AdaRound, BRECQ, AWQ, SmoothQuant, GPTQ, HAWQ-V2, ZeroQ), all adapted using branch-aware quantization. Experiments are implemented in PyTorch with a unified, configuration-driven QuantKAN codebase, and all non-quantization settings are held fixed for fair comparison; full architectural details and hyperparameters are provided in the appendix D.

## 5. Results and Analysis

### 5.1. KAN Performance with Quantization-Aware Training (QAT)

Table 1 reports the top-3 quantization-aware training (QAT) methods for each architecture and dataset, selected based on their robustness under progressively lower bit-precision. To ensure a fair and concise comparison in the main paper, LSQ and LSQ+ are treated as a single method family, and only the stronger variant is retained when both appear among the top performers. The selection emphasizes stability at low-bit regimes, including w3, w2, and joint weight–activation quantization, where performance degradation is most pronounced for spline-based models. For completeness and

Table 1. Top-3 QAT methods per architecture, selected based on robustness under low-bit precision. When both LSQ and LSQ+ rank among the top performers, only the stronger variant is retained. Complete results are reported in Table 10.

Dataset	Architecture	Method	w32a32	w8	w4	w3	w2	w4a4	w3a3	w2a2
MNIST	KAN FCN	DSQ	98.00	98.43	98.24	98.13	97.71	97.71	97.82	97.71
		LSQ+	98.00	98.24	98.13	98.03	97.79	97.87	97.73	96.97
		PACT	98.00	98.17	98.14	98.07	97.21	97.77	97.64	96.09
	KAN ConvNet	DoReFa	95.70	95.41	95.67	95.17	93.55	91.09	91.08	88.52
		DSQ	95.70	95.81	95.44	95.62	89.54	90.40	90.14	89.54
		LSQ+	95.70	95.70	95.56	95.17	94.46	90.95	94.11	92.04
	KAGN Simple	DoReFa	98.67	98.70	98.71	98.58	98.33	97.93	97.96	96.22
		DSQ	98.67	98.43	98.24	98.64	85.14	96.66	93.28	85.14
		LSQ	98.67	98.95	98.69	98.74	98.34	86.25	78.42	76.32
CIFAR-10	KAGN Simple	DSQ	62.24	62.77	62.88	61.31	45.44	48.60	48.33	45.44
		DoReFa	62.24	62.84	61.68	58.88	55.87	50.01	47.38	37.15
		LSQ	62.24	62.74	61.74	61.70	56.03	28.27	30.48	29.24
	KAGN Simple (8L)	DSQ	78.10	72.22	76.86	77.36	39.44	50.64	48.05	39.44
		LSQ	78.10	76.00	75.49	73.21	72.10	46.41	47.67	47.38
		DoReFa	78.10	76.87	70.27	64.99	52.49	49.79	38.00	30.57
	KAGN Simple (8L V2)	DSQ	68.06	67.12	68.03	67.54	43.10	34.01	35.45	43.10
		LSQ	68.06	67.20	65.87	68.49	68.41	52.36	53.01	47.00
		DoReFa	68.06	67.93	66.89	53.58	23.39	29.49	9.66	8.62
CIFAR-100	VGG-like KAGN V2	DSQ	58.77	57.82	58.58	58.23	1.00	56.81	55.86	1.00
		LSQ+	58.77	58.05	56.98	1.00	30.18	1.00	1.00	1.01
		DoReFa	58.77	58.50	48.96	1.00	21.61	18.37	1.00	1.08

transparency, the full set of QAT results across all methods, architectures, and precision settings is provided in Table 10.

**Observation 1: Across all datasets and architectures, DSQ consistently emerges as the most robust QAT method, particularly under aggressive low-bit settings.** DSQ either matches or exceeds full-precision accuracy at moderate bit-widths and exhibits a markedly more graceful degradation as precision is reduced. This behavior is especially evident for deeper and more structured KAN variants (e.g., KAGN Simple (8L) and CIFAR-100 models), suggesting that DSQ’s smooth, differentiable quantization formulation aligns well with the continuous and highly non-linear nature of spline-based layers.

**Observation 2: The LSQ/LSQ+ family remains competitive at moderate precision,** often achieving strong performance at w8 and w4 across architectures (Table 1). Robustness degrades at very low precision, particularly under joint weight–activation quantization (w4a4 and below), where several models show sharp accuracy drops. LSQ+ is retained only when it improves stability, indicating that its added flexibility is beneficial but not consistently reliable across KAN/KAGN variants. On CIFAR-100, LSQ+ is especially hyperparameter-sensitive: with default settings it can collapse at low bit widths, but training from scratch with tuned hyperparameters recovers reasonable accuracy, suggesting an optimization issue.

**Observation 3: DoReFa consistently ranks among the top-3 methods for simpler or moderately deep architectures, especially on MNIST and CIFAR-10.** While it does not always achieve the highest accuracy at higher precision, DoReFa demonstrates comparatively stable behavior under low-bit weight quantization and remains competitive when other methods experience catastrophic failure. This makes DoReFa a strong and reliable baseline for KAN-based models where simplicity and robustness are prioritized.

In contrast, other QAT approaches such as PACT and QIL (reported in Table 10) frequently exhibit *catastrophic collapse at low precision*, particularly under joint weight–activation quantization, and are therefore excluded from the main-paper comparison. These failures highlight the limitations of conventional clipping- or interval-based quantization schemes when applied directly to spline-based architectures.

Overall, these results indicate that **structure-aware and smooth quantization schemes are critical for KANs**, especially as model depth and dataset complexity increase. The consistent dominance of DSQ across architectures and datasets motivates its use as a default QAT strategy for low-precision deployment of KAN models, while LSQ/LSQ+ and DoReFa serve as competitive alternatives depending on precision targets and architectural constraints.

**Large-scale validation.** To assess whether the observed QAT trends extend to more challenging regimes, Table 2 reports top-performing QAT methods on TinyImageNet and ImageNet using deep VGG-style KAGN architectures. Despite the increased dataset complexity and depth, DSQ remains the most robust method across all evaluated precisions, consistently matching or exceeding full-precision accuracy at moderate bit-widths and degrading gracefully under joint quantization. LSQ+ remains competitive at higher precision but exhibits sharper degradation under aggressive joint quantization, while DoReFa shows reasonable stability at weight-only low precision but degrades more rapidly when activations are quantized. These results confirm that the advantages of smooth, structure-aware quantization persist at scale, reinforcing DSQ as a reliable default for low-bit deployment of deep KAN models.

Table 2. Top QAT methods under low-bit precision for large-scale datasets. FP denotes full precision (w32a32).

Dataset / Arch.	Method	FP	w8	w4	w3	w4a4
TinyImageNet	DSQ		44.21	44.10	44.70	43.90
	LSQ+	42.64	43.29	43.90	43.78	30.25
	DoReFa		45.07	43.02	40.55	35.05
ImageNet	DSQ	61.15	60.93	61.39	60.47	55.19
	LSQ+		60.01	55.13	42.98	29.28

## 5.2. KAN Performance with Post-Training Quantization

Table 3 summarizes the performance of representative post-training quantization (PTQ) methods across multiple KAN architectures and datasets. For clarity in the main paper, we focus on the four strongest PTQ approaches: GPTQ, AdaRound, AWQ, and BRECQ, selected based on robustness under reduced bit precision and consistency across architectures. The complete PTQ results, including additional baselines and all precision settings, are reported in Appendix 11.

**Observation 4: Across all datasets, GPTQ consistently emerges as the most reliable PTQ method, achieving near full-precision accuracy at w8 and w4 and exhibiting the most graceful degradation as precision is reduced.** This trend holds for both shallow and deep KAN variants, indicating that second-order error compensation is particularly effective for spline-based architectures, even without re-training. However, at extreme low-bit settings (e.g., w2 or joint quantization), GPTQ still experiences noticeable accuracy degradation, highlighting the inherent limitations of calibration-only approaches.

**Observation 5: AdaRound and AWQ form a second tier of competitive PTQ methods, performing well at moderate precision (w8 and w4) but degrading more rapidly as bit-width decreases.** AdaRound generally outperforms AWQ at lower precisions, suggesting that learned rounding

decisions provide greater robustness than activation-aware scaling alone. Nonetheless, both methods struggle under joint weight–activation quantization, especially for deeper KAN models and more complex datasets such as CIFAR-100.

**Observation 6: BRECQ exhibits mixed but notable behavior.** While it underperforms GPTQ and AdaRound on simpler architectures, it remains comparatively robust for convolutional and VGG-like KAN variants, occasionally outperforming other PTQ methods under joint quantization. This suggests that block-wise reconstruction can partially mitigate quantization error in structured architectures, albeit with limited stability at very low bit-widths.

In contrast, other PTQ baselines such as Uniform quantization, HAWQ-V2, and ZeroQ (see Table 11) frequently exhibit *severe performance collapse* under low-bit or joint quantization. These failures are particularly pronounced for deeper KAN models, underscoring the sensitivity of spline-based networks to unstructured or poorly calibrated quantization schemes.

*Overall*, these results indicate that while PTQ can be effective for KANs at moderate precision, *its reliability deteriorates rapidly as bit-width decreases*, especially for deeper architectures and joint quantization. Compared to QAT, PTQ methods lack the ability to adapt spline parameters during training, making them less suitable for aggressive low-bit deployment of KAN models. This performance gap motivates the use of quantization-aware strategies, particularly for applications requiring extreme compression or hardware-constrained inference.

## 5.3. Quantization Design Analysis Across KAN Variants

In Table 4 and Figure 4, we summarize average marginal effects of (i) granularity (per-channel vs. per-tensor), (ii) symmetry (symmetric vs. asymmetric), and (iii) quantization target (weights vs. activations), aggregated over bit-widths and quantizers on CIFAR-10 (full results in Appendix Table 12 and 13). For *activation* quantization, per-channel scaling consistently improves accuracy across variants, with the largest gain for PyKAN ( $\Delta_{\text{ch-t}}^{(A)} = +0.20$ ). In contrast, for *weight* quantization, per-channel scaling is variant-dependent and can be harmful: EfficientKAN and PyKAN are insensitive, while FastKAN degrades substantially ( $\Delta_{\text{ch-t}}^{(W)} = -0.74$ ), suggesting poorly conditioned channel-wise weight scales. The effect of symmetric vs. asymmetric quantization is smaller and variant-dependent, indicating interaction with layer formulation. Finally, target sensitivity varies by variant: EfficientKAN and PyKAN slightly favor activation quantization, whereas FastKAN and GramLayer favor weight quantization on average.

Table 3. Top-4 PTQ methods per architecture, selected based on robustness under reduced precision. Complete PTQ results are provided in Appendix Table 11.

Dataset	Architecture	Method	w32a32	w8	w4	w3	w2	w4a4	w3a3	w2a2
MNIST	KAN FCN	GPTQ	97.99	98.00	97.86	97.07	76.58	95.88	88.99	40.90
		AdaRound	97.99	97.97	97.78	96.36	42.87	95.75	88.88	32.35
		AWQ	97.99	97.98	97.80	95.53	33.65	95.55	88.73	21.02
		BRECQ	97.99	73.77	72.58	73.60	50.51	70.87	86.93	52.38
CIFAR-10	KAN ConvNet	GPTQ	95.69	95.69	95.65	95.63	88.18	10.10	10.10	10.10
		AdaRound	95.69	95.69	95.61	95.20	80.03	9.73	10.28	10.25
		AWQ	95.69	95.68	95.62	95.01	62.70	10.10	10.10	10.32
		BRECQ	95.69	36.37	37.79	30.31	35.07	75.60	93.52	64.97
CIFAR-100	KAGN Simple	GPTQ	98.66	98.65	97.96	90.11	27.39	97.96	90.11	27.39
		AdaRound	98.66	98.76	96.59	88.41	29.83	96.59	88.41	29.83
		AWQ	98.66	98.70	97.35	57.65	13.36	97.35	57.65	13.36
		BRECQ	98.66	98.73	96.11	76.07	23.33	96.22	81.70	12.80
CIFAR-10	KAGN Simple	GPTQ	62.23	62.36	56.52	40.85	11.68	56.52	40.85	11.68
		AdaRound	62.23	62.27	53.92	34.21	11.61	53.92	34.21	11.61
		AWQ	62.23	62.17	54.01	22.01	9.58	54.01	22.01	9.58
		BRECQ	62.23	62.28	52.28	24.47	12.35	49.98	27.43	16.21
CIFAR-100	KAGN Simple (8L)	GPTQ	78.08	78.02	69.13	41.59	9.92	69.13	41.59	9.92
		AdaRound	78.08	78.15	61.57	37.93	10.09	61.57	37.93	10.09
		AWQ	78.08	77.92	60.17	28.01	12.17	60.17	28.01	12.17
		BRECQ	78.08	77.88	60.28	27.64	12.82	62.28	39.31	19.20
CIFAR-100	KAGN Simple (8L V2)	GPTQ	68.09	68.05	13.47	2.65	1.14	13.47	2.65	1.14
		AdaRound	68.09	67.67	2.77	1.01	1.00	2.77	1.01	1.00
		AWQ	68.09	67.62	3.74	1.00	1.00	3.74	1.00	1.00
		BRECQ	68.09	67.57	3.86	1.00	1.00	3.12	1.49	1.47
CIFAR-100	VGG-like KAGN V2	GPTQ	58.70	58.23	39.73	14.23	1.98	39.57	13.26	0.99
		AdaRound	58.70	55.91	22.66	6.05	1.47	22.63	5.46	1.03
		AWQ	58.70	58.30	29.57	13.44	1.22	29.44	12.48	1.15
		BRECQ	58.70	58.29	29.80	15.64	1.88	32.17	15.99	2.57

Table 4. Ablation summary on CIFAR-10: average marginal effects of quantization design choices across bit-widths and methods. Positive values indicate higher accuracy. Full results are reported in Appendix.

Variant	$\Delta_{\text{ch-t}}^{(W)}$	$\Delta_{\text{ch-t}}^{(A)}$	$\Delta_{\text{sym-asym}}^{(W)}$	$\Delta_{\text{sym-asym}}^{(A)}$	$\Delta_{\text{w-a}}$
eff-kan	-0.00	+0.07	-0.06	+0.03	-0.01
fastkan	-0.74	+0.10	+0.12	-0.15	+0.17
gramlayer	-0.12	+0.10	-0.20	-0.07	+0.15
pykan	-0.00	+0.20	+0.00	-0.02	-0.05

#### 5.4. Parameter Sensitivity and Mixed-Precision Design

We probe which KAN parameter groups are most vulnerable to low precision using a single-parameter mixed-precision ablation: for each variant, we quantize exactly one parameter group to  $b \in \{2, 3, 4\}$  bits while keeping the remaining groups at 8-bit, and measure degradation  $\Delta(p, b) = \max(0, \text{Acc}_{\text{FP}} - \text{Acc}_q(p=b))$ . Table 5 reports, for each dataset/variant/quantizer, the most sensitive group aggregated over  $b \in \{2, 3, 4\}$  (mean and worst-case degradation; full breakdown is in the Appendix Table 14).

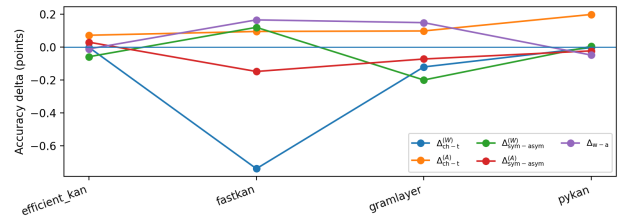


Figure 4. CIFAR-10 ablation summary across KAN variants. We plot average marginal effects aggregated over bit-widths and quantizers:  $\Delta_{\text{ch-t}}^{(W/A)}$  compares per-channel vs. per-tensor scaling for weights/activations,  $\Delta_{\text{sym-asym}}^{(W/A)}$  compares symmetric vs. asymmetric quantization, and  $\Delta_{\text{w-a}}$  compares weight vs. activation sensitivity. Positive values indicate higher accuracy.

Across both datasets, DSQ is consistently robust, with near-zero degradation in almost all cases. In contrast, LSQ exhibits clear parameter dependence on CIFAR-10: basis/spline-related groups dominate sensitivity (FASTKAN  $w_{\text{spline}}$ : mean  $\Delta=1.37$ , max  $\Delta=3.07$ ; GRAM  $w_{\text{gram}}$ : mean  $\Delta=1.80$ , max  $\Delta=2.62$ ), while scaling-like parameters show substantially smaller degradation (e.g., PyKAN  $w_{\text{scale}, \text{base}}$ :

**Table 5.** Most sensitive parameter group under single-parameter mixed precision, where one parameter group is quantized while all others remain at 8-bit. Degradation is defined as  $\Delta = \max(0, \text{Acc}_{\text{FP}} - \text{Acc})$ . **Data:** C10=CIFAR-10, MN=MNIST. **Var.:** EFF=EfficientKAN, FST=FastKAN, GRM=GRAM, PYK=PyKAN. **Sensitive:**  $w_b$ =base weights,  $w_s$ =spline/basis weights,  $w_g$ =gram weights,  $w_c$ =coefficient weights,  $w_{sb}$ =base scaling weights.

Data	Variant	Qtz.	Param	Mean $\Delta$	Max $\Delta$	Base Acc.
C10	EFF	DSQ	$w_b$	0.00	0.00	49.21
C10	EFF	LSQ	$w_b$	0.14	0.43	49.21
C10	FST	DSQ	$w_b$	0.00	0.00	39.30
C10	FST	LSQ	$w_s$	1.37	3.07	39.30
C10	GRM	DSQ	$w_b$	0.17	0.36	49.83
C10	GRM	LSQ	$w_g$	1.80	2.62	49.83
C10	PYK	DSQ	$w_c$	0.00	0.00	49.95
C10	PYK	LSQ	$w_{sb}$	0.33	0.66	49.95
MN	EFF	DSQ	$w_b$	0.00	0.00	97.82
MN	EFF	LSQ	$w_b$	0.27	0.74	97.82
MN	FST	DSQ	$w_b$	0.00	0.00	97.36
MN	FST	LSQ	$w_b$	0.05	0.14	97.36
MN	GRM	DSQ	$w_b$	0.00	0.00	98.00
MN	GRM	LSQ	$w_b$	0.28	0.48	98.00
MN	PYK	DSQ	$w_c$	0.00	0.00	97.53
MN	PYK	LSQ	$w_{sb}$	0.11	0.30	97.53

mean  $\Delta=0.33$ ). Sensitivity is markedly weaker on MNIST, suggesting that parameter fragility emerges primarily under harder regimes. These findings motivate QuantKAN mixed precision: preserve higher precision for the most sensitive basis/spline parameters and aggressively quantize the remaining groups to improve efficiency with minimal accuracy loss.

**From sensitivity to mixed precision.** The observed parameter-wise sensitivity directly suggests a simple and effective mixed-precision policy. For each KAN variant, we retain higher precision (8 bit) for the most sensitive parameter group, identified by the largest mean degradation  $\Delta$  under single parameter quantization, and quantize the remaining groups more aggressively when their degradation is small. Table 6 summarizes the resulting recommendations for CIFAR-10 under LSQ, where parameter sensitivity is most pronounced. Across variants, fragile basis or spline-related parameters consistently require higher precision, while scaling or auxiliary parameters tolerate lower bit-widths with minimal accuracy loss. This yields an actionable design rule for QuantKAN: allocate precision where it matters most, while compressing the remaining parameters to improve efficiency with negligible performance impact.

For clarity, parameter groups  $(A, B, C)$  correspond to variant-specific weights: EfficientKAN ( $w_{\text{base}}, w_{\text{spline}}, w_{\text{scaler}}$ ), FastKAN ( $w_{\text{base}}, w_{\text{spline}}$ ), GRAM ( $w_{\text{base}}, w_{\text{gram}}, w_{\text{beta}}$ ), and PyKAN

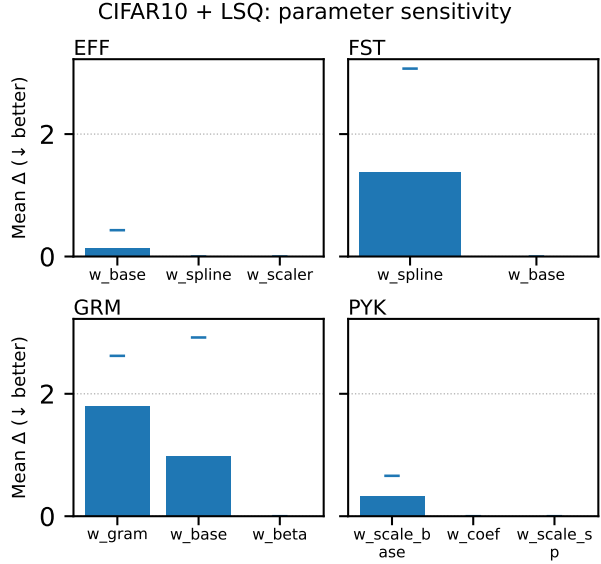


**Figure 5. CIFAR-10 + LSQ parameter-wise sensitivity under single-parameter mixed precision.** Bars show mean degradation  $\Delta = \max(0, \text{Acc}_{\text{FP}} - \text{Acc})$  averaged over  $b \in \{2, 3, 4\}$  when quantizing one parameter group and keeping others at 8-bit; markers indicate worst-case degradation. Lower is better.

**Table 6.** Mixed-precision recommendations derived from parameter sensitivity on CIFAR-10 under LSQ. For each KAN variant, the most sensitive parameter group (highest mean degradation  $\Delta$ ) is retained at 8-bit, while remaining groups are quantized more aggressively when degradation is small (lower  $\Delta$  is better). Parameter groups follow the variant-specific ordering  $(A, B, C)$  defined below.

Variant	Bits (A/B/C)	Most sensitive	Mean $\Delta$	Max $\Delta$
EfficientKAN	A8/B2/C2	A ( $w_{\text{base}}$ )	0.14	0.43
FastKAN	A2/B8	B ( $w_{\text{spline}}$ )	1.37	3.07
GRAM	A4/B8/C2	B ( $w_{\text{gram}}$ )	1.80	2.62
PyKAN	A2/B8/C2	B ( $w_{\text{scale,base}}$ )	0.33	0.66

$(w_{\text{coef}}, w_{\text{scale,base}}, w_{\text{scale,sp}})$ .

## 6. Conclusion

We present **QuantKAN**, the first unified framework for quantizing Kolmogorov–Arnold Networks under both QAT and PTQ. By explicitly modeling the dual-branch structure of KAN layers, QuantKAN adapts a broad set of modern quantizers to spline- and polynomial-based components and establishes the first systematic low-bit benchmarks across datasets and KAN variants. Our results show that KANs can remain accurate at low precision when quantization is co-designed with KAN structure: DSQ is the most robust choice for aggressive QAT, while GPTQ is strongest among PTQ methods at moderate precision. Ablations further reveal strong parameter-wise sensitivity, often concentrated in spline/basis components, motivating mixed-precision policies that allocate bits where they matter most. Overall,

QuantKAN provides practical tooling and design guidelines for efficient, hardware-friendly deployment of spline-based networks.

## Impact Statement

This work aims to advance efficient and interpretable machine learning by introducing a unified framework for quantizing Kolmogorov–Arnold Networks (KANs). QuantKAN enables reduced-precision inference for spline- and polynomial-based layers, which can reduce memory and compute requirements and may broaden the feasibility of using KANs in resource-constrained settings and specialized hardware implementations.

QuantKAN is a general-purpose model compression and evaluation toolkit, not an application-specific system. It does not introduce new data sources, learning objectives, or deployment contexts beyond those common in quantization research. The broader impacts therefore mirror those of efficiency methods in general: improved efficiency can facilitate wider deployment of ML models, and any downstream harms (e.g., unfair or privacy-invasive uses) depend on how models are applied. These considerations motivate standard responsible-use practices, including appropriate task selection, evaluation for bias and failure modes, and compliance with relevant policies.

Overall, we anticipate the primary impact to be enabling more accessible experimentation and use of spline-based models under realistic compute and memory constraints.

## References

Bhalgat, Y., Lee, J., Nagel, M., Blankevoort, T., and Kwak, N. Lsq+: Improving low-bit quantization through learnable offsets and better initialization, 2020. URL <https://arxiv.org/abs/2004.09576>.

Blealtan and Dash, A. efficient-kan. <https://github.com/Blealtan/efficient-kan>, 2024. GitHub repository.

Cai, Y., Yao, Z., Dong, Z., Gholami, A., Mahoney, M. W., and Keutzer, K. Zeroq: A novel zero shot quantization framework, 2020. URL <https://arxiv.org/abs/2001.00281>.

Choi, J., Wang, Z., Venkataramani, S., Chuang, P. I.-J., Srinivasan, V., and Gopalakrishnan, K. Pact: Parameterized clipping activation for quantized neural networks, 2018. URL <https://arxiv.org/abs/1805.06085>.

Dong, Z., Yao, Z., Cai, Y., Arfeen, D., Gholami, A., Mahoney, M. W., and Keutzer, K. Hawq-v2: Hessian aware trace-weighted quantization of neural networks, 2019a. URL <https://arxiv.org/abs/1911.03852>.

Dong, Z., Yao, Z., Gholami, A., Mahoney, M., and Keutzer, K. Hawq: Hessian aware quantization of neural networks with mixed-precision, 2019b. URL <https://arxiv.org/abs/1905.03696>.

Drokin, I. Kolmogorov-arnold convolutions: Design principles and empirical studies, 2024. URL <https://arxiv.org/abs/2407.01092>.

Esser, S. K., McKinstry, J. L., Bablani, D., Appuswamy, R., and Modha, D. S. Learned step size quantization, 2020. URL <https://arxiv.org/abs/1902.08153>.

Frantar, E., Ashkboos, S., Hoefer, T., and Alistarh, D. Gptq: Accurate post-training quantization for generative pre-trained transformers, 2023. URL <https://arxiv.org/abs/2210.17323>.

Gholami, A., Kim, S., Dong, Z., Yao, Z., Mahoney, M. W., and Keutzer, K. A survey of quantization methods for efficient neural network inference, 2021. URL <https://arxiv.org/abs/2103.13630>.

Gong, R., Liu, X., Jiang, S., Li, T., Hu, P., Lin, J., Yu, F., and Yan, J. Differentiable soft quantization: Bridging full-precision and low-bit neural networks, 2019. URL <https://arxiv.org/abs/1908.05033>.

Jacob, B., Kligys, S., Chen, B., Zhu, M., Tang, M., Howard, A., Adam, H., and Kalenichenko, D. Quantization and training of neural networks for efficient integer-arithmetic-only inference, 2017. URL <https://arxiv.org/abs/1712.05877>.

Jung, S., Son, C., Lee, S., Son, J., Kwak, Y., Han, J.-J., Hwang, S. J., and Choi, C. Learning to quantize deep networks by optimizing quantization intervals with task loss, 2018. URL <https://arxiv.org/abs/1808.05779>.

Khochawongwat, T. Gram: Kan meets gram polynomials. <https://github.com/Khochawongwat/GRAMKAN>, 2024. GitHub repository.

Li, Y., Gong, R., Tan, X., Yang, Y., Hu, P., Zhang, Q., Yu, F., Wang, W., and Gu, S. Brecq: Pushing the limit of post-training quantization by block reconstruction, 2021. URL <https://arxiv.org/abs/2102.05426>.

Li, Z. Kolmogorov-arnold networks are radial basis function networks, 2024. URL <https://arxiv.org/abs/2405.06721>.

Lin, J., Tang, J., Tang, H., Yang, S., Chen, W.-M., Wang, W.-C., Xiao, G., Dang, X., Gan, C., and Han, S. Awq: Activation-aware weight quantization for llm compression and acceleration, 2024. URL <https://arxiv.org/abs/2306.00978>.

Liu, Z., Wang, Y., Vaidya, S., Ruehle, F., Halverson, J., Soljačić, M., Hou, T. Y., and Tegmark, M. Kan: Kolmogorov-arnold networks, 2025. URL <https://arxiv.org/abs/2404.19756>.

Nagel, M., Amjad, R. A., van Baalen, M., Louizos, C., and Blankevoort, T. Up or down? adaptive rounding for post-training quantization, 2020. URL <https://arxiv.org/abs/2004.10568>.

Xiao, G., Lin, J., Seznec, M., Wu, H., Demouth, J., and Han, S. Smoothquant: Accurate and efficient post-training quantization for large language models, 2024. URL <https://arxiv.org/abs/2211.10438>.

Yu, R., Yu, W., and Wang, X. Kan or mlp: A fairer comparison, 2024. URL <https://arxiv.org/abs/2407.16674>.

Zhou, S., Wu, Y., Ni, Z., Zhou, X., Wen, H., and Zou, Y. Dorefa-net: Training low bitwidth convolutional neural networks with low bitwidth gradients, 2018. URL <https://arxiv.org/abs/1606.06160>.

## Appendix Contents

This appendix provides supporting analyses and implementation details for QUANTKAN. Appendix A characterizes branch-specific weight distributions across major KAN variants and relates them to the sensitivity trends discussed in the main paper. Appendices B and C give implementation-aligned formulations and pseudocode for the QAT quantizers and PTQ methods evaluated in our experiments. Appendix D lists the full experimental and quantization hyperparameters used for fair comparisons. Finally, Appendix E reports complete parameter-wise sensitivity results that motivate our mixed-precision and branch-aware design choices.

- Appendix A: Weight Distribution Analysis (Section A)
- Appendix B: QAT Quantizers (Section B)
- Appendix C: PTQ Methods (Section C)
- Appendix D: Experimental Hyperparameters (Section D)
- Appendix E: Additional Parameter Sensitivity Results (Section E)

## A. Weight Distribution Analysis Across KAN Variants

This appendix provides a comprehensive analysis of weight distributions across four major KAN architectures: PyKAN, EfficientKAN, FastKAN, and GRAM-KAN. All models were trained on MNIST with identical hyperparameters (2-layer networks, 64 hidden units). Understanding these distributions, in conjunction with the parameter sensitivity analysis in Section 5.4, informed the design of our branch-aware quantization framework.

### A.1. Summary of Distributional Patterns

Table 7 presents detailed statistics for base and spline weights across all variants. Two patterns emerge that are relevant for quantization:

1. **Base weights consistently exhibit heavier tails.** Across all four variants, base weights show higher kurtosis ( $\kappa$ ) than spline weights, ranging from  $\kappa = 4.3$  (GRAM-KAN) to  $\kappa = 37.0$  (EfficientKAN). This indicates the presence of outliers that would dominate min-max calibration.
2. **Dynamic range relationships vary by architecture.** While base weights have heavier tails, the relationship between branch ranges differs: EfficientKAN base weights span  $4\times$  the range of spline weights, whereas FastKAN shows the opposite pattern with spline weights spanning  $2\times$  the base range.

**Important:** These distributional statistics alone do not predict quantization sensitivity. Our parameter sensitivity analysis (Section 5.4) reveals that *spline and basis parameters are more sensitive to quantization error than base weights*, despite often having narrower distributions. This counterintuitive finding underscores the importance of empirical sensitivity analysis over distribution-based heuristics.

*Table 7.* Weight distribution statistics across KAN variants (MNIST, 2-layer networks). Kurtosis ( $\kappa$ ) measures tail heaviness (Gaussian:  $\kappa = 3$ ); range denotes the 1st–99th percentile span. Note: distributional width does not directly predict quantization sensitivity—see Section 5.4 for sensitivity analysis.

Variant	Base weights ( $W_b$ )			Spline weights ( $W_s$ )		
	$\kappa$	$\sigma$	range	$\kappa$	$\sigma$	range
PyKAN	36.0	0.047	0.240	2.7	0.041	0.184
EfficientKAN	37.0	0.047	0.236	8.2	0.011	0.057
FastKAN	20.6	0.038	0.200	3.0	0.096	0.447
GRAM-KAN	4.3	0.050	0.167	5.2	0.026	0.097

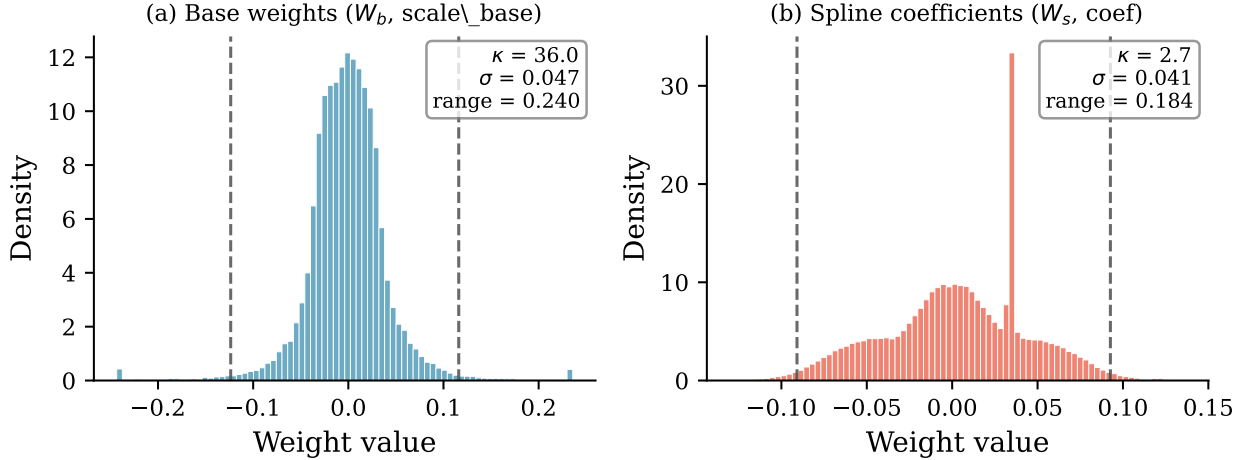


Figure 6. Weight distributions in trained PyKAN. (a) Base weights (`scale_base`) show heavy tails ( $\kappa = 36.0$ ) with outliers beyond  $\pm 0.25$ . (b) Spline coefficients (`coef`) are near-Gaussian ( $\kappa = 2.7$ ) with a sharp peak. Dashed lines: 1st/99th percentiles.

## A.2. PyKAN

PyKAN (Liu et al., 2025) uses B-spline basis functions with learnable coefficients. The base branch applies a scaling factor (`scale_base`) to a SiLU activation, while the spline branch combines B-spline coefficients (`coef`) with a separate scaling term (`scale_sp`).

Figure 6 shows the weight distributions. Base weights exhibit pronounced heavy tails ( $\kappa = 36.0$ ) with outliers at approximately  $\pm 0.25$ , while spline coefficients follow a near-Gaussian distribution ( $\kappa = 2.7$ ) with a characteristic sharp peak near zero. The spline distribution shows slight positive skew and a distinct mode around 0.05, reflecting the learned basis function structure.

### Quantization implications:

- Base weights require outlier-robust calibration (99th percentile) due to heavy tails
- Despite narrower distribution, `scale_base` parameters show moderate sensitivity under LSQ (mean  $\Delta = 0.33$ , max  $\Delta = 0.66$  on CIFAR-10)
- DSQ achieves near-zero degradation across all parameter groups, making it the recommended QAT method for PyKAN

## A.3. EfficientKAN

EfficientKAN (Blealtan & Dash, 2024) reimplements KANs for computational efficiency using matrix operations. It maintains explicit `base_weight` and `spline_weight` tensors with an optional `spline_scaler`.

Figure 7 reveals the most extreme distributional contrast among the variants studied. Base weights have the highest kurtosis ( $\kappa = 37.0$ ) with substantial outliers, while spline weights are highly concentrated ( $\kappa = 8.2$ ,  $\sigma = 0.011$ ) with a dynamic range only one-quarter that of base weights.

### Quantization implications:

- The  $4 \times$  range difference makes shared quantization particularly harmful
- Spline weights' narrow distribution ( $\sigma = 0.011$ ) might suggest easy quantization, but `base_weight` actually shows the highest sensitivity under LSQ (mean  $\Delta = 0.14$ , max  $\Delta = 0.43$  on CIFAR-10)
- Mixed-precision policy: retain 8-bit for `base_weight`, aggressively quantize `spline_weight` and `spline_scaler`

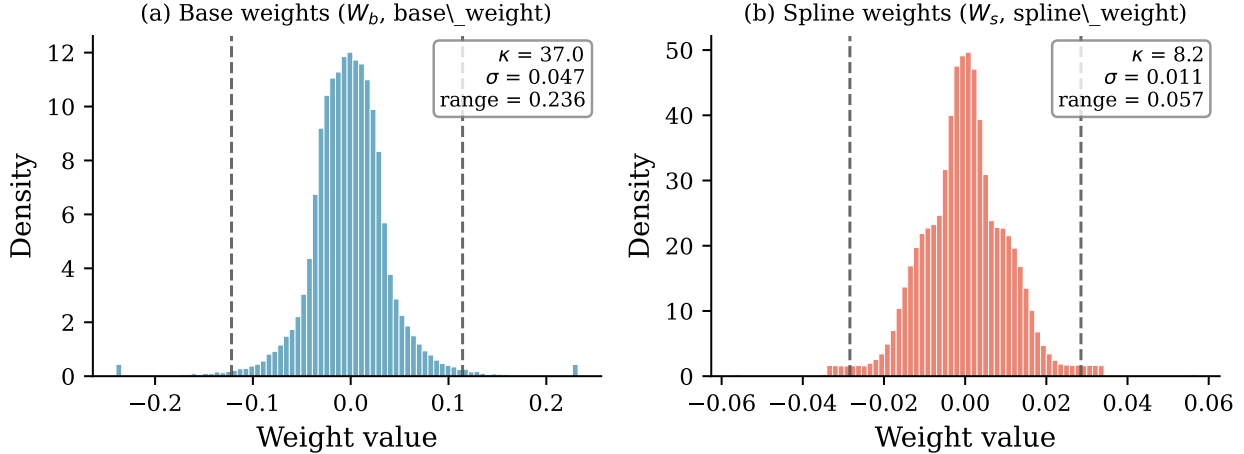


Figure 7. Weight distributions in trained EfficientKAN. (a) Base weights show the heaviest tails among all variants ( $\kappa = 37.0$ ). (b) Spline weights are highly concentrated ( $\sigma = 0.011$ ) with  $4\times$  smaller dynamic range.

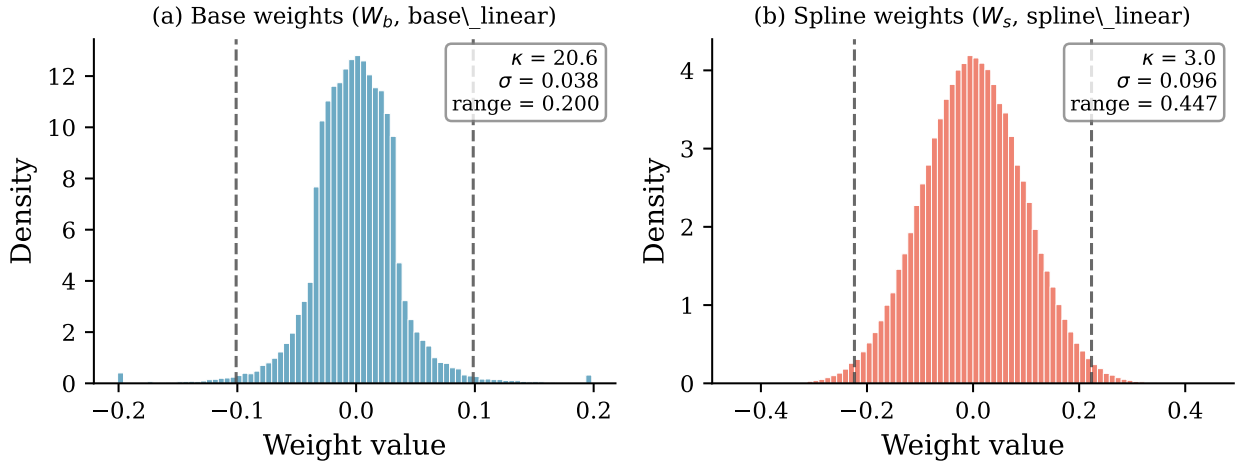


Figure 8. Weight distributions in trained FastKAN. (a) Base weights exhibit moderate heavy tails ( $\kappa = 20.6$ ). (b) Spline weights are near-Gaussian ( $\kappa = 3.0$ ) but span  $2\times$  the dynamic range of base weights. Despite wider range, spline weights show the highest quantization sensitivity among all variants.

#### A.4. FastKAN

FastKAN (Li, 2024) replaces B-splines with radial basis functions (RBFs) for faster computation. The architecture uses standard linear layers for both branches: `base_linear` and `spline_linear`.

Figure 8 shows a pattern distinct from other variants. While base weights exhibit elevated kurtosis ( $\kappa = 20.6$ ), spline weights are nearly Gaussian ( $\kappa = 3.0$ ) but with a substantially *wider* dynamic range—approximately  $2\times$  that of base weights.

#### Quantization implications:

- FastKAN exhibits the highest parameter sensitivity among all variants: `spline_linear` weights show mean  $\Delta = 1.37$ , max  $\Delta = 3.07$  under LSQ on CIFAR-10
- **Critical:** Per-channel weight quantization is harmful for FastKAN ( $\Delta_{\text{ch-t}}^{(W)} = -0.74$ ), unlike other variants—use per-tensor weight scaling
- Mixed-precision policy: retain 8-bit for `spline_linear`, quantize `base_linear` aggressively

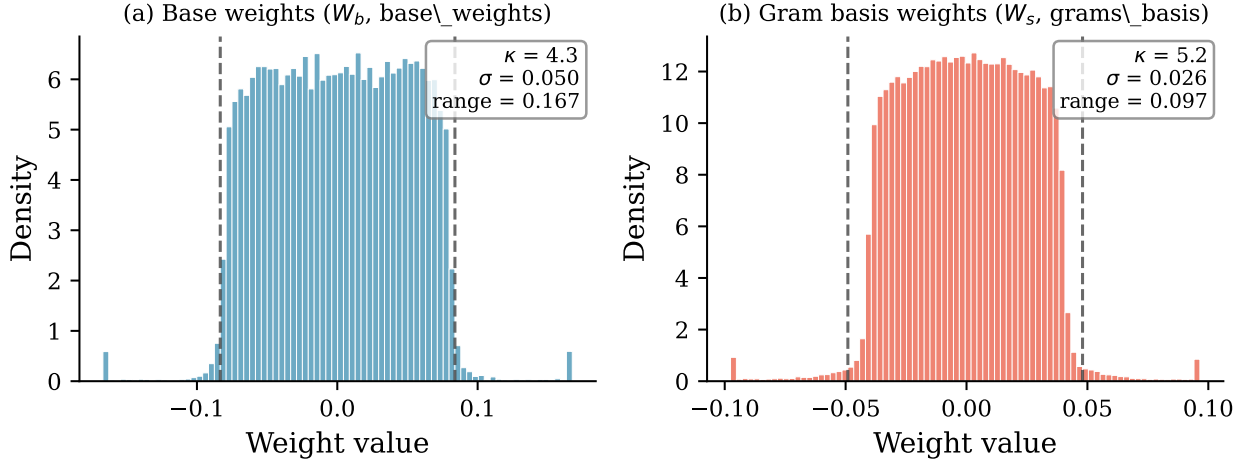


Figure 9. Weight distributions in trained GRAM-KAN. (a) Base weights show near-uniform distribution with low kurtosis ( $\kappa = 4.3$ ). (b) Gram basis weights have moderate kurtosis ( $\kappa = 5.2$ ). Despite similar scales, basis weights are highly sensitive to quantization.

### A.5. GRAM-KAN

GRAM-KAN (Drokin, 2024) uses Gram polynomial basis functions instead of splines. The base branch uses `base_weights`, while the polynomial branch uses `grams_basis_weights` organized by polynomial degree.

Figure 9 shows the most uniform distributions among the variants. Base weights have the lowest kurtosis ( $\kappa = 4.3$ ), only slightly above Gaussian, with a notably flat-topped shape. Gram basis weights show moderate kurtosis ( $\kappa = 5.2$ ) with a more peaked distribution. Both branches have relatively similar scales.

#### Quantization implications:

- Lower kurtosis in both branches reduces outlier sensitivity compared to other variants
- Despite similar scales, `grams_basis_weights` show high sensitivity under LSQ (mean  $\Delta = 1.80$ , max  $\Delta = 2.62$  on CIFAR-10)—the second-highest among all variants
- Mixed-precision policy: retain 8-bit for `grams_basis_weights`, quantize `base_weights` to 4-bit, `beta_weights` to 2-bit
- GRAM-KAN benefits most from DSQ, which achieves near-zero degradation across all parameters

### A.6. Summary: Distribution vs. Sensitivity

In all variants except EfficientKAN, the most sensitive parameter group is *not* the one with the widest distribution or heaviest tails.

This finding has important practical implications:

1. **Do not rely solely on distributional statistics** for calibration decisions. Sensitivity analysis (as in Section 5.4) provides more actionable guidance.
2. **Spline/basis parameters generally require higher precision** despite often having narrower distributions. This likely reflects the functional importance of accurate basis representations for KAN expressivity.
3. **Smooth quantization methods (DSQ) are more robust** across all variants and parameter groups, achieving near-zero degradation where step-size methods (LSQ) show significant sensitivity variation.

### A.7. Detailed Statistics

For completeness, Table 8 provides extended statistics including skewness, interquartile range, and parameter counts.

Table 8. Extended weight statistics across KAN variants.

Variant	Branch	Count	$\mu$	$\sigma$	Skew	$\kappa$	IQR
PyKAN	Base	50,816	-0.001	0.047	-0.48	36.0	0.054
	Spline	457,344	0.004	0.041	-0.19	2.7	0.058
EfficientKAN	Base	50,816	-0.002	0.047	-0.37	37.0	0.053
	Spline	457,344	0.000	0.011	0.03	8.2	0.013
FastKAN	Base	50,890	0.000	0.038	-0.31	20.6	0.045
	Spline	406,528	0.000	0.096	0.00	3.0	0.130
GRAM-KAN	Base	50,816	0.000	0.050	0.08	4.3	0.086
	Spline	203,272	0.000	0.026	-0.01	5.2	0.042

### A.8. Calibration Recommendations

Based on both distributional analysis and sensitivity results, Table 9 provides architecture-specific calibration and precision recommendations.

Table 9. Recommended quantization strategies by KAN variant, informed by both distributional analysis (this appendix) and parameter sensitivity (Section 5.4).

Variant	Recommended QAT	Mixed-precision (base/spline)	Per-ch. weights?
PyKAN	DSQ	2-bit / 8-bit	Safe
EfficientKAN	DSQ or LSQ	8-bit / 2-bit	Safe
FastKAN	DSQ	2-bit / 8-bit	Avoid
GRAM-KAN	DSQ	4-bit / 8-bit	Safe

The key takeaway is that **DSQ is the safest default** across all variants, achieving robust performance without requiring careful per-variant tuning. When using LSQ or other step-size methods, practitioners should (1) prioritize precision for spline/basis parameters, (2) avoid per-channel weight quantization for FastKAN, and (3) expect higher sensitivity on complex datasets (CIFAR-10/100) compared to simpler benchmarks (MNIST).

## B. Quantization-Aware Training (QAT) Quantizers

This appendix provides a concise and implementation-aligned description of the QAT quantizers used in our framework: LSQ, LSQ+, DoReFa, DSQ, QIL, and PACT. We present each method with (i) core equations, (ii) pseudocode that matches our implementation choices, and (iii) brief guidance on when the method is especially effective for KAN/KAGN-style models.

### B.1. Preliminaries: Fake-Quantization and STE Primitives

We adopt the standard *fake-quantization* view: in the forward pass, tensors are quantized to an integer grid and dequantized back to floating point; in the backward pass, we use Straight-Through Estimators (STE) to preserve gradient flow through discrete operations.

Let bit-width be  $b$ , integer range be  $(q_{\min}, q_{\max})$ , and step size (scale) be  $s > 0$ . For signed quantization we commonly use  $q_{\max} = 2^{b-1} - 1$ ; for unsigned we use  $q_{\max} = 2^b - 1$  with  $q_{\min} = 0$ . We use  $\text{clip}(x, a, b)$  for clamping.

Our implementation uses compile-friendly STE helpers:

$$\text{round\_ste}(x) = (\lfloor x \rfloor - x)_{\text{stopgrad}} + x, \quad (5)$$

$$\text{sign\_ste}(x) = (\text{sign}(x) - x)_{\text{stopgrad}} + x, \quad (6)$$

and for LSQ-style step-size stabilization, a gradient scaling helper:

$$\text{grad\_scale}(x, g) = (x - xg)_{\text{stopgrad}} + xg. \quad (7)$$

KAN/KAGN layers often combine linear mixing with nonlinear function blocks (e.g., basis expansions). This can produce

heterogeneous per-channel statistics, skewed intermediate distributions, and occasional outliers. The quantizers below are chosen to address these failure modes via (i) learned step sizes (LSQ), (ii) learned offsets (LSQ+), (iii) bounded transforms (DoReFa), (iv) smoother discretization (DSQ), (v) learned prune/clip intervals (QIL), and (vi) learned activation clipping (PACT).

## B.2. LSQ: Learned Step Size Quantization

LSQ learns the step size  $s$  by optimizing task loss through a uniform quantizer (Esser et al., 2020). For a tensor  $x$  (weights or activations),

$$x_q = \text{clip}\left(\left\lfloor \frac{x}{s} \right\rfloor, q_{\min}, q_{\max} \right), \quad \hat{x} = x_q \cdot s. \quad (8)$$

The rounding uses STE, and the gradient of  $s$  is stabilized via `grad_scale`, with a scale factor typically proportional to  $1/\sqrt{N \cdot q_{\max}}$  (per-tensor or per-channel), as in LSQ.

Learning  $s$  using task loss tends to outperform fixed calibration at low bit-widths, and per-channel  $s$  can accommodate heterogeneous channel scales.

---

### Algorithm 1 LSQ fake-quantization (implementation-aligned)

---

**Require:** Tensor  $x$ , bits  $b$ , flags: `all_positive`, `symmetric`, `per_channel`, axis `ch_axis`

- 1: Set  $(q_{\min}, q_{\max})$  from flags (unsigned or signed; strict symmetric optional).
- 2: Initialize learnable step  $s$  (per-tensor or per-channel), e.g.  $s_0 \propto \mathbb{E}|x|/\sqrt{q_{\max}}$ .
- 3: Compute gradient scale  $g \leftarrow 1/\sqrt{N_{\text{per-scale}} q_{\max}}$ .
- 4:  $s \leftarrow \text{grad\_scale}(\max(s, \varepsilon), g)$
- 5:  $u \leftarrow x/s$
- 6:  $u \leftarrow \text{clip}(u, q_{\min}, q_{\max})$
- 7:  $x_q \leftarrow \text{round\_ste}(u)$
- 8: **return**  $\hat{x} \leftarrow x_q \cdot s$

---

LSQ is a strong default for weight and activation QAT when uniform hardware-friendly levels are desired but ranges vary across layers/channels (common in KAN coefficient tensors).

## B.3. LSQ+: Learned Step Size and Offset (Asymmetric Quantization)

LSQ+ extends LSQ by learning an offset (zero-point-like) term to better fit skewed distributions (Bhalgat et al., 2020). In its general form,

$$x_q = \text{clip}\left(\left\lfloor \frac{x - \beta}{s} \right\rfloor, n, p \right), \quad \hat{x} = x_q \cdot s + \beta. \quad (9)$$

In our implementation, we store a learnable offset  $z$  in the integer domain and use an affine form in scaled coordinates. A practical detail in our code is to avoid trivial gradient cancellation through the de-offset step by detaching the dequant offset term in the final reconstruction (this preserves stable learning of  $z$  in practice).

---

### Algorithm 2 LSQ+ fake-quantization (implementation-aligned)

---

**Require:** Tensor  $x$ , bits  $b$ , learnable  $(s, z)$ , integer range  $(q_{\min}, q_{\max})$

- 1:  $s \leftarrow \text{grad\_scale}(\max(s, \varepsilon), g_s)$ ;  $z \leftarrow \text{grad\_scale}(z, g_z)$
- 2:  $z_{\text{eff}} \leftarrow \text{clip}(z, q_{\min}, q_{\max})$  {forward clamp}
- 3:  $q_{\text{pre}} \leftarrow x/s + z_{\text{eff}}$
- 4:  $q_{\text{int}} \leftarrow \text{round\_ste}(\text{clip}(q_{\text{pre}}, q_{\min}, q_{\max}))$
- 5:  $z_{\text{ng}} \leftarrow \text{stopgrad}(z_{\text{eff}})$  {prevents gradient cancellation}
- 6: **return**  $\hat{x} \leftarrow (q_{\text{int}} - z_{\text{ng}}) \cdot s$

---

LSQ+ is especially helpful for activations that are skewed or shifted. This often arises in nonlinear function blocks where the output distribution is not centered around zero.

#### B.4. DoReFa: Bounded Transforms + Uniform Discretization

DoReFa-Net proposes low-bit quantization via simple bounded transforms followed by uniform discretization (Zhou et al., 2018). Our implementation is QAT-ready and back-compatible, supporting: (i)  $b = 32$  identity, (ii) special  $b = 1$  behavior, (iii) per-channel weight stats, and (iv) optional stochastic gradient quantization hooks.

**Activation quantization.** We assume/clamp activations to  $[0, 1]$ . For  $b \geq 2$ ,

$$\hat{a} = \text{clip}\left(\frac{\text{round\_ste}(a \cdot n)}{n}, 0, 1\right), \quad n = 2^b - 1, \quad (10)$$

and for  $b = 1$  we use a 0.5 threshold with STE.

**Weight quantization (our exact behavior).** Let  $w_t = \tanh(w)$ .

- $b = 1$ : binary weights with learned magnitude  $E = \mathbb{E}|w_t|$  (per-channel or per-tensor, detached),

$$\hat{w} = \text{sign\_ste}(w_t) \cdot E.$$

- $b \geq 2$ : compute  $m = \max|w_t|$  (per-channel or per-tensor, detached), map to  $[0, 1]$  via  $w_{01} = \text{clip}(w_t/(2m) + 1/2, 0, 1)$ , quantize  $w_{01}$  uniformly, then map back:

$$\hat{w} = (2\hat{w}_{01} - 1) \cdot m.$$

---

#### Algorithm 3 DoReFa fake-quantization (matches provided implementation)

---

**Require:** Tensor  $x$ , bits  $b$ , mode  $\in \{\text{weight, activation}\}$ , flags: `per_channel, ch_axis`

```

1: if  $b = 32$  then
2:   return  $x$ 
3: end if
4: if mode=weight then
5:    $x_t \leftarrow \tanh(x)$ 
6:   if  $b = 1$  then
7:      $E \leftarrow \mathbb{E}(|x_t|)$  (detached; per-channel if enabled)
8:     return  $\text{sign\_ste}(x_t) \cdot E$ 
9:   else
10:     $m \leftarrow \max(|x_t|)$  (detached; per-channel if enabled)
11:     $w_{01} \leftarrow \text{clip}(x_t/(2m) + 0.5, 0, 1)$ 
12:     $n \leftarrow 2^b - 1$ 
13:     $\hat{w}_{01} \leftarrow \text{clip}(\text{round\_ste}(w_{01} \cdot n)/n, 0, 1)$ 
14:    return  $\hat{x} \leftarrow (2\hat{w}_{01} - 1) \cdot m$ 
15:  end if
16: else
17:    $a_{01} \leftarrow \text{clip}(x, 0, 1)$ 
18:   if  $b = 1$  then
19:      $y \leftarrow \mathbb{I}[a_{01} \geq 0.5]$ 
20:     return  $(y - a_{01})_{\text{stopgrad}} + a_{01}$ 
21:   else
22:      $n \leftarrow 2^b - 1$ 
23:     return  $\text{clip}(\text{round\_ste}(a_{01} \cdot n)/n, 0, 1)$ 
24:   end if
25: end if

```

---

DoReFa can be a strong stability anchor at low bit-width because  $\tanh(\cdot)$  bounds weights and scaling uses detached per-channel statistics. This can help prevent runaway scales in deep stacks.

### B.5. DSQ: Differentiable Soft Quantization

DSQ replaces hard rounding with a differentiable soft staircase controlled by a sharpness parameter, bridging full precision and low-bit training (Gong et al., 2019). The sharpness is typically annealed so that soft rounding becomes closer to hard rounding later in training.

---

**Algorithm 4** DSQ fake-quantization (implementation-aligned structure)

**Require:** Tensor  $x$ , bits  $b$ , bounds (unsigned or symmetric), sharpness  $\alpha$

- 1: Clamp  $x$  to a bounded interval (unsigned or symmetric depending on mode)
- 2: Map to quant units:  $t \leftarrow (x - \ell)/s$  (unsigned) or  $t \leftarrow x/s$  (symmetric)
- 3: Soft-round:  $t \leftarrow \text{SoftRound}(t; \alpha)$
- 4: Clamp  $t$  to  $[q_{\min}, q_{\max}]$
- 5: **return** Dequantize:  $\hat{x} \leftarrow t \cdot s + \ell$  (unsigned) or  $\hat{x} \leftarrow t \cdot s$  (symmetric)

---

DSQ is useful when hard rounding + STE causes brittle optimization at very low bit-width (e.g., 2–3 bits), particularly when quantization noise is amplified by nonlinear function blocks.

### B.6. QIL: Quantization Interval Learning (Pruning + Clipping + Discretization)

QIL learns a quantization interval and reshapes values into a bounded range before discretization (Jung et al., 2018). It can explicitly *prune* small magnitudes (map to 0) and *clip* large magnitudes (map to  $\pm 1$ ), while learning an internal mapping controlled by  $(c, d, \gamma)$ :

$$v(w) = \begin{cases} 0, & |w| < c - d, \\ \text{sign}(w), & |w| > c + d, \quad \alpha = \frac{1}{2d}, \beta = -\frac{c}{2d} + \frac{1}{2}, \\ (\text{clip}(\alpha|w| + \beta, 0, 1))^{\gamma} \text{sign}(w), & \text{otherwise}, \end{cases} \quad (11)$$

We then discretize on a uniform grid. Our implementation uses a safe minimum of one positive level for weights at very low bits, i.e.,  $q = \max(2^{b-1} - 1, 1)$ .

---

**Algorithm 5** QIL fake-quantization (implementation-aligned)

**Require:** Tensor  $x$ , bits  $b$ , mode  $\in \{\text{weight, activation}\}$ , learned  $(c, d)$ , optional  $\gamma$

- 1: Parameterize  $d > 0$  and  $c \geq d$  (e.g., softplus); compute  $\alpha \leftarrow 1/(2d)$ ,  $\beta \leftarrow -c/(2d) + 1/2$
- 2: **if** mode=weight **then**
- 3:    $a \leftarrow |x|$ ,  $s \leftarrow \text{sign}(x)$
- 4:    $m \leftarrow \text{clip}(\alpha a + \beta, 0, 1)$ ; optionally  $m \leftarrow m^{\gamma}$
- 5:    $v \leftarrow 0$  if  $a < c - d$ ;  $v \leftarrow s$  if  $a > c + d$ ; **else**  $v \leftarrow m \cdot s$
- 6:    $q \leftarrow \max(2^{b-1} - 1, 1)$
- 7:   **return**  $\hat{x} \leftarrow (\text{round\_ste}(|v|q)/q) \cdot \text{sign}(v)$
- 8: **else**
- 9:    $u \leftarrow 0$  if  $x < c - d$ ;  $u \leftarrow 1$  if  $x > c + d$ ; **else**  $u \leftarrow \text{clip}(\alpha x + \beta, 0, 1)$
- 10:    $q \leftarrow 2^b - 1$
- 11:   **return**  $\hat{x} \leftarrow \text{round\_ste}(uq)/q$
- 12: **end if**

---

QIL can be effective when tensors have many small values plus a few large outliers, because the learned interval can prune noise and clip extremes. However, at very low bits, it can be higher-variance than LSQ/PACT unless interval learning is well regularized.

### B.7. PACT: Parameterized Clipping Activation

PACT learns a clipping threshold  $\alpha$  to reduce activation range and improve effective resolution (Choi et al., 2018). After clipping, it applies uniform quantization:

$$x_c = \text{clip}(x, 0, \alpha), \quad \Delta = \alpha/(2^b - 1), \quad \hat{x} = \Delta \cdot \text{clip}(\lfloor x_c/\Delta \rfloor, 0, 2^b - 1). \quad (12)$$

Our implementation also supports a symmetric extension  $x_c = \text{clip}(x, -\alpha, \alpha)$  for signed tensors, with  $\Delta = \alpha/(2^{b-1} - 1)$ .

---

**Algorithm 6** PACT fake-quantization (implementation-aligned)

---

**Require:** Tensor  $x$ , bits  $b$ , learned clip  $\alpha$ , flag `symmetric`

- 1: Ensure  $\alpha > 0$  (e.g., softplus +  $\varepsilon$  or clamp)
- 2: **if** `symmetric` **then**
- 3:    $q_{\max} \leftarrow 2^{b-1} - 1$ ,  $q_{\min} \leftarrow -2^{b-1}$  (or strict variant)
- 4:    $x_c \leftarrow \text{clip}(x, -\alpha, \alpha)$ ;  $\Delta \leftarrow \alpha/q_{\max}$
- 5: **else**
- 6:    $q_{\max} \leftarrow 2^b - 1$ ,  $q_{\min} \leftarrow 0$
- 7:    $x_c \leftarrow \text{clip}(x, 0, \alpha)$ ;  $\Delta \leftarrow \alpha/q_{\max}$
- 8: **end if**
- 9:  $q \leftarrow \text{round\_ste}(x_c/\Delta)$
- 10:  $q \leftarrow \text{clip}(q, q_{\min}, q_{\max})$
- 11: **return**  $\hat{x} \leftarrow q \cdot \Delta$

---

PACT is a strong choice for activation quantization when rare outliers otherwise force a large range and poor resolution. Learning  $\alpha$  shrinks the range and often stabilizes low-bit activation quantization in nonlinear blocks.

### B.8. Summary: Which Quantizer When (Practical, KAN/KAGN-Oriented)

A practical, implementation-consistent rule-set for KAN/KAGN is:

- **Default:** LSQ for weights (per-channel, symmetric), LSQ or LSQ+ for activations depending on skew.
- **Skewed activations:** prefer LSQ+ (learned offset) to better use available levels.
- **Outlier-dominated activations:** prefer PACT (learned clipping).
- **Unstable low-bit training (2–3 bits):** consider DSQ for smoother optimization.
- **Heavy-tailed / many small coefficients:** consider QIL (learned interval with pruning+clipping), but expect higher variance without regularization.
- **Stable, minimal baseline:** DoReFa (bounded tanh weights + detached per-channel scaling) can remain stable when learned-parameter quantizers are fragile.

## C. Post-Training Quantization (PTQ) Methods

This appendix presents the post-training quantization (PTQ) methods used in this work. Each method is described using (i) a mathematical formulation that characterizes the quantization objective, and (ii) an implementation-aligned pseudo-code block. Unlike quantization-aware training (QAT), PTQ methods do not update model parameters via backpropagation; instead, they rely on calibration data and analytical or optimization-based criteria to reduce quantization error.

### C.1. Preliminaries

Let  $W \in \mathbb{R}^{d_{\text{out}} \times d_{\text{in}}}$  denote a floating-point weight tensor and  $X \in \mathbb{R}^{d_{\text{in}} \times n}$  denote calibration inputs. Uniform affine quantization maps  $W$  to

$$\hat{W} = s \cdot \text{clip}\left(\left\lfloor \frac{W}{s} \right\rfloor, q_{\min}, q_{\max}\right), \quad (13)$$

where  $s$  is a scale and  $[q_{\min}, q_{\max}]$  defines the integer range. All PTQ methods discussed below modify either the rounding operator, the scaling strategy, or the objective used to select  $\hat{W}$ .

KAN models introduce additional challenges for PTQ due to heterogeneous parameter groups (base weights, spline coefficients, polynomial kernels) and non-uniform activation distributions, motivating structure-aware and sensitivity-aware PTQ.

## C.2. Uniform PTQ

Uniform PTQ applies Eq. (13) directly using min–max calibrated scales. Each weight element is quantized independently, without considering the effect of quantization error on the layer output. For symmetric quantization, the scale is computed as

$$s = \frac{\max |W|}{2^{b-1} - 1}. \quad (14)$$

---

**Algorithm 7** Uniform PTQ (implementation-aligned)

**Require:** Weight tensor  $W$ , bits  $b$ , flag `symmetric`

- 1: **if** symmetric **then**
- 2:    $q_{\max} \leftarrow 2^{b-1} - 1$ ,  $q_{\min} \leftarrow -2^{b-1}$
- 3:    $s \leftarrow \max |W|/q_{\max}$
- 4: **else**
- 5:    $q_{\max} \leftarrow 2^b - 1$ ,  $q_{\min} \leftarrow 0$
- 6:    $s \leftarrow (\max W - \min W)/q_{\max}$
- 7: **end if**
- 8:  $q \leftarrow \text{round}(W/s)$
- 9:  $q \leftarrow \text{clip}(q, q_{\min}, q_{\max})$
- 10: **return**  $\hat{W} \leftarrow q \cdot s$

---

Uniform PTQ is computationally efficient and stable for KAN base weights, but it often produces large functional errors for spline or polynomial parameters with heavy-tailed distributions.

## C.3. AdaRound

AdaRound improves upon uniform rounding by optimizing rounding decisions using calibration data. Instead of immediately applying  $\lfloor \cdot \rfloor$ , AdaRound introduces learnable rounding offsets  $\alpha$  and defines

$$\hat{W} = s \cdot \left( \left\lfloor \frac{W}{s} \right\rfloor + \sigma(\alpha) \right), \quad (15)$$

where  $\sigma(\cdot)$  is a sigmoid function. The offsets  $\alpha$  are optimized to minimize output reconstruction error

$$\min_{\alpha} \|WX - \hat{W}X\|_2^2. \quad (16)$$

---

**Algorithm 8** AdaRound PTQ (layer-wise reconstruction)

**Require:** Weight tensor  $W$ , calibration inputs  $X$ , bits  $b$ , iterations  $T$

- 1: Initialize scale  $s$  and rounding parameters  $\alpha$
- 2: **for**  $t = 1$  to  $T$  **do**
- 3:    $\hat{W} \leftarrow s \cdot (\lfloor W/s \rfloor + \sigma(\alpha))$
- 4:   Compute  $\|WX - \hat{W}X\|_2^2$
- 5:   Update  $\alpha$
- 6: **end for**
- 7: Finalize rounding decisions
- 8: **return**  $\hat{W}$

---

AdaRound is particularly effective for spline coefficients and polynomial kernels in KANs, where naive rounding can distort learned functional relationships.

## C.4. GPTQ and GPTQ-Strict

GPTQ minimizes a second-order approximation of quantization error by incorporating Hessian information estimated from calibration data. The quantization objective is

$$\mathcal{L}_{\text{GPTQ}} = (W - \hat{W})^\top H(W - \hat{W}), \quad (17)$$

where  $H$  is a Hessian or Hessian proxy of the loss with respect to  $W$ . Weights are quantized sequentially, and the error introduced by early decisions is compensated by updating remaining weights.

---

**Algorithm 9** GPTQ PTQ (block-wise Hessian-aware)

**Require:** Weight matrix  $W$ , calibration inputs  $X$ , block size  $B$ , damping  $\lambda$

- 1: Estimate Hessian proxy  $H \approx 2XX^\top + \lambda I$
- 2: Compute Cholesky factorization of  $H^{-1}$
- 3: **for** each block of columns **do**
- 4:   **for** each column  $j$  in block **do**
- 5:     Quantize  $W_{:,j}$  to  $\hat{W}_{:,j}$
- 6:     Propagate error using  $H^{-1}$
- 7:   **end for**
- 8: **end for**
- 9: **return**  $\hat{W}$

---

The GPTQ-Strict variant enforces a fixed triangular update order, improving numerical stability and determinism. GPTQ is especially effective for large KAN mixing matrices and spline tensors.

### C.5. BRECQ

BRECQ reconstructs quantized blocks by minimizing output reconstruction error on calibration data. For a block with inputs  $X^{(i)}$  and outputs  $Y^{(i)}$ , BRECQ optimizes

$$\min_{\hat{W}^{(i)}} \|Y^{(i)} - \hat{W}^{(i)} X^{(i)}\|_2^2. \quad (18)$$

---

**Algorithm 10** BRECQ PTQ (block reconstruction)

**Require:** Block weights  $W^{(i)}$ , cached inputs  $X^{(i)}$ , outputs  $Y^{(i)}$ , iterations  $T$

- 1: **for**  $t = 1$  to  $T$  **do**
- 2:   Quantize block weights  $\hat{W}^{(i)}$
- 3:   Compute  $\|Y^{(i)} - \hat{W}^{(i)} X^{(i)}\|_2^2$
- 4:   Update quantization parameters
- 5: **end for**
- 6: **return**  $\hat{W}^{(i)}$

---

BRECQ is well-suited for structured KAN blocks when targeting extremely low precision (e.g., INT2/INT3).

### C.6. AWQ

AWQ reduces quantization error by rescaling weights using activation statistics. Given calibration activations  $A$ , AWQ computes a per-channel scaling factor

$$\gamma = \mathbb{E}[|A|], \quad (19)$$

and rescales weights as  $\tilde{W} = W/\gamma$  prior to quantization.

---

**Algorithm 11** AWQ PTQ (activation-aware scaling)

**Require:** Weights  $W$ , calibration activations  $A$ , bits  $b$

- 1:  $\gamma \leftarrow \mathbb{E}[|A|]$
- 2:  $\tilde{W} \leftarrow W/\gamma$
- 3: Apply uniform PTQ to  $\tilde{W}$
- 4: **return**  $\hat{W}$

---

AWQ is particularly effective for spline-based KAN layers, where a small number of channels dominate activation magnitude.

### C.7. HAWQ-V2

HAWQ-V2 assigns mixed precision using layer-wise sensitivity estimates based on the Hessian trace. The trace is approximated using Hutchinson’s estimator:

$$\text{Tr}(H) \approx \mathbb{E}_r[r^\top H r], \quad (20)$$

where  $r$  is a random Rademacher vector.

---

**Algorithm 12** HAWQ-V2 mixed-precision PTQ

**Require:** Model layers  $\{\ell\}$ , calibration data

- 1: **for** each layer  $\ell$  **do**
- 2:   Estimate  $\text{Tr}(H_\ell)$
- 3: **end for**
- 4: Allocate bit-widths based on sensitivity
- 5: **return** Mixed-precision configuration

---

KAN layers exhibit heterogeneous sensitivity due to nonlinear basis functions, making Hessian-aware bit allocation particularly effective.

### C.8. SmoothQuant

SmoothQuant reduces activation outliers by redistributing scale between weights and activations. Given a smoothing factor  $\alpha$ , it applies

$$W' = W \cdot \alpha, \quad A' = A/\alpha, \quad (21)$$

followed by quantization of  $W'$  and  $A'$ .

---

**Algorithm 13** SmoothQuant PTQ (scale redistribution)

**Require:** Weights  $W$ , activations  $A$ , smoothing factor  $\alpha$

- 1:  $W' \leftarrow W \cdot \alpha$
- 2:  $A' \leftarrow A/\alpha$
- 3: Quantize  $W'$  and  $A'$
- 4: **return** Quantized model

---

This approach is especially beneficial when spline activations exhibit heavy-tailed distributions.

### C.9. ZeroQ

ZeroQ enables data-free PTQ by synthesizing calibration inputs that match internal statistics. Synthetic inputs  $X_{\text{syn}}$  are optimized to minimize

$$\mathcal{L}_{\text{syn}} = \|\mu(X_{\text{syn}}) - \mu_{\text{ref}}\|_2^2 + \|\sigma(X_{\text{syn}}) - \sigma_{\text{ref}}\|_2^2. \quad (22)$$

---

**Algorithm 14** ZeroQ data-free PTQ

**Require:** Model, reference statistics

- 1: Initialize synthetic inputs
- 2: Optimize inputs to match statistics
- 3: Apply PTQ using synthetic data
- 4: **return** Quantized model

---

## D. Experimental Hyperparameters

This appendix summarizes the hyperparameters used across all experiments. All runs are configuration-driven, and unless otherwise stated, hyperparameters are held fixed across quantization methods to ensure fair comparison.

## D.1. Datasets and Preprocessing

**MNIST.** Images are normalized using mean 0.1307 and standard deviation 0.3081. During training, we apply random rotation (up to  $10^\circ$ ); evaluation uses deterministic normalization only. Input resolution is  $28 \times 28$  (single channel).

**CIFAR-10 and CIFAR-100.** We use standard data augmentation including random horizontal flip, AutoAugment (CIFAR10 / ImageNet / SVHN policies), and TrivialAugmentWide. Inputs are normalized to mean 0.5 and standard deviation 0.5 per channel. Evaluation uses deterministic normalization without augmentation.

**TinyImageNet.** Images are resized and cropped to  $64 \times 64$  resolution. Training uses random crop with padding 4, random horizontal flip, and AutoAugment (ImageNet policy). Evaluation uses resize followed by center crop. ImageNet normalization statistics are applied.

**ImageNet.** Training uses random resized crop ( $224 \times 224$ ), random horizontal flip, and AutoAugment (ImageNet policy). Evaluation uses resize to 256 followed by center crop to 224. Standard ImageNet normalization is applied. Class indices are remapped to preserve the canonical 0–999 label space.

## D.2. Model Architectures

We evaluate KAN backbones that appear in Table 10, spanning both fully connected and convolutional designs:

- **Fully connected KAN:** **KAN FCN**, implemented with variant-specific spline layers (EfficientKAN-style KANLinear, FastKANLayer, GRMLayer, and PyKANLayer) in a two-layer MLP for MNIST/CIFAR-scale inputs.
- **Convolutional KAN:** **KAN ConvNet**, a shallow CNN that replaces standard convolutions and classifiers with KAN convolution blocks (KAN\_Convolutional\_Layer) and KANLinear heads; we use dataset-specific instantiations (e.g., KANConvNet\_MNIST, KANConvNet\_CIFAR10).
- **Convolutional KAGN:** **KAGN Simple** and **KAGN Simple 8 Layers**, implemented as SimpleConvKAGN and EightSimpleConvKAGN with stacked KAGNConv2DLayer blocks followed by global pooling and a KAGN/linear classifier head. For CIFAR-10 we evaluate both the 4-block “Simple” configuration and the 8-layer configuration.
- **VGG-like KAGN:** **VGG Like KAGN V2**, implemented via vggkagn (VGG11v2-style configuration) with KAGNConv2DLayer features, adaptive pooling, and a linear classifier head. We use this VGG-like KAGN only for CIFAR-100 as reported in Table 10. These VGG-like KAGN models are adopted directly from (Drokin, 2024).

Unless stated otherwise, the fully connected **KAN FCN** models use two spline-based layers (input  $\rightarrow$  hidden  $\rightarrow$  output), with hidden width set per dataset (e.g., 64 for MNIST and up to 256 for CIFAR-scale inputs). The **KAN ConvNet** models are shallow backbones with KAN convolution blocks, max-pooling between stages, and a KANLinear classifier. **KAGN Simple** uses four KAGN convolution blocks with downsampling and global pooling, while **KAGN Simple 8 Layers** deepens this design to eight KAGN convolution blocks. The **VGG Like KAGN V2** backbone follows a VGG11-style stage pattern with KAGN convolution blocks and max-pooling, ending with adaptive pooling and a linear classifier.

## D.3. Optimization and Training

**Optimizer.** All models are trained using Adam or AdamW with default  $\beta$  parameters ( $\beta_1 = 0.9$ ,  $\beta_2 = 0.999$ ). Weight decay is set to  $10^{-4}$  for CIFAR-scale and larger datasets, and disabled for MNIST unless otherwise noted.

**Learning rate.** The base learning rate is selected per dataset scale:

- MNIST:  $1 \times 10^{-3}$
- CIFAR-10/100:  $1 \times 10^{-3}$  to  $3 \times 10^{-4}$
- TinyImageNet / ImageNet:  $3 \times 10^{-4}$

Learning rate schedules follow cosine decay or step decay as specified in the configuration files.

**Batch size.** Batch size is dataset-dependent:

- MNIST: 128–256
- CIFAR-10/100: 128
- TinyImageNet: 128
- ImageNet: 64

**Epochs.** Models are trained for:

- MNIST: 20–40 epochs
- CIFAR-10/100: 200 epochs
- TinyImageNet: 100 epochs
- ImageNet: 90 epochs

Early stopping is applied only for selected MNIST runs.

#### D.4. Quantization-Aware Training (QAT)

**Bit-widths.** We evaluate weight-only and joint weight–activation quantization at  $\{8, 4, 3, 2\}$  bits.

**Quantizer configuration.** Unless otherwise stated:

- Base weights, spline/basis weights, and activations use **independent quantizers**
- Activations default to asymmetric quantization
- Weights default to symmetric quantization
- Per-tensor scaling is used by default; per-channel scaling is evaluated in ablations

#### Method-specific settings.

- **LSQ / LSQ+**: step sizes initialized from running statistics; LSQ+ uses learnable zero-points
- **PACT**: clipping thresholds initialized uniformly and learned per branch
- **QIL**: interval centers and widths initialized from min–max statistics
- **DSQ**: temperature parameter initialized to a low value and annealed during training
- **DoReFa**: fixed tanh-based normalization (no learnable parameters)

#### D.5. Post-Training Quantization (PTQ)

**Calibration.** Unless stated otherwise, PTQ uses 512–2048 calibration samples drawn from the training set. For data-free methods, synthetic inputs are generated following the original method specifications.

### Method-specific settings.

- **AdaRound**: soft-to-hard rounding with cosine annealing
- **BRECQ**: block-wise reconstruction with joint branch calibration
- **AWQ**: per-channel activation-aware scaling applied independently per branch
- **SmoothQuant**: activation scaling folded into weights, applied separately to base and spline/basis pathways
- **GPTQ**: damped least-squares optimization with branch-specific curvature estimation
- **HAWQ-V2**: Hessian trace estimation with sub-weight-level bit allocation
- **ZeroQ**: synthetic calibration using  $TV + \ell_2$  regularization

### D.6. Reproducibility

All experiments use deterministic data loading when enabled, fixed random seeds, and identical pretrained checkpoints across quantization methods. The full set of configuration files used in this work is included with the codebase to enable exact reproduction of all reported results.

**Full ablation tables.** Tables 12 and 13 report exhaustive CIFAR-10 results. Rows index (variant, bit-width), and columns enumerate symmetry–granularity settings for each quantizer.

**Granularity heatmaps.** Figures 10–11 report  $\Delta_{ch-t}$ , the accuracy change from per-tensor to per-channel scaling (positive favors per-channel), averaged over symmetric/asymmetric ranges. This isolates granularity sensitivity across quantizers and bit-widths for each KAN variant.

## E. Additional Parameter Sensitivity Results

This appendix provides the full parameter-wise sensitivity results that underlie the summary and design recommendations presented in the main paper. Specifically, we report the degradation incurred when quantizing a single parameter group to low precision while keeping all remaining parameters at 8-bit.

Table 14 report mean degradation  $\Delta = \max(0, \text{Acc}_{FP} - \text{Acc})$  for each parameter group and bit-width  $b \in \{2, 3, 4\}$  on CIFAR-10 and MNIST, respectively. Lower values indicate greater robustness to quantization. These detailed results support the main paper’s conclusions regarding parameter sensitivity and the resulting mixed-precision design strategy.

Table 10. Accuracy (%) of QAT methods on different datasets under various bit-precision settings. (**w4** means **w4a32**, likewise **w3=w3a32**, **w2=w2a32**).

Architecture	Method	w32a32	w8	w4	w3	w2	w4a4	w3a3	w2a2
MNIST dataset									
KAN FCN	LSQ	98.00	98.22	98.11	98.00	97.55	97.94	97.70	96.76
	LSQ+		98.24	98.13	98.03	97.79	97.87	97.73	96.97
	DoReFa		98.19	98.14	97.96	97.63	95.82	95.62	94.95
	DSQ		98.43	98.24	98.13	97.71	97.71	97.82	97.71
	PACT		98.17	98.14	98.07	97.21	97.77	97.64	96.09
	QIL		98.30	98.04	97.37	93.15	97.61	95.95	22.17
KAN ConvNet	LSQ	95.70	18.53	94.00	94.40	94.95	92.44	91.35	90.78
	LSQ+		11.35	95.56	95.17	94.46	90.95	94.11	92.04
	DoReFa		95.41	95.67	95.17	93.55	91.09	91.08	88.52
	DSQ		95.81	95.44	95.62	89.54	90.40	90.14	89.54
	PACT		95.12	94.28	91.07	11.35	94.39	90.25	11.35
	QIL		94.34	93.03	87.86	11.35	93.17	91.74	11.35
KAGN Simple	LSQ	98.67	98.95	98.69	98.74	98.34	86.25	78.42	76.32
	LSQ+		97.15	98.49	98.50	98.35	89.03	88.33	91.93
	DoReFa		98.70	98.71	98.58	98.33	97.93	97.96	96.22
	DSQ		98.43	98.24	98.64	85.14	96.66	93.28	85.14
	PACT		98.24	98.61	97.63	11.35	98.36	94.93	11.35
	QIL		98.80	98.76	97.76	75.85	85.56	28.29	11.35
CIFAR-10 dataset									
KAGN Simple	LSQ	62.24	62.74	61.74	61.70	56.03	28.27	30.48	29.24
	LSQ+		62.03	61.38	60.90	58.26	29.23	29.30	29.14
	DoReFa		62.84	61.68	58.88	55.87	50.01	47.38	37.15
	DSQ		62.77	62.88	61.31	45.44	48.60	48.33	45.44
	PACT		59.58	54.15	40.94	10.00	37.64	26.14	10.00
	QIL		61.57	49.76	35.57	10.00	28.23	14.35	10.00
KAGN Simple 8 Layers	LSQ	78.10	76.00	75.49	73.21	72.10	46.41	47.67	47.38
	LSQ+		70.27	74.71	75.10	72.24	47.47	46.15	39.65
	DoReFa		76.87	70.27	64.99	52.49	49.79	38.00	30.57
	DSQ		72.22	76.86	77.36	39.44	50.64	48.05	39.44
	PACT		76.60	70.22	10.00	10.00	50.39	10.00	10.00
	QIL		77.31	71.93	52.95	10.00	39.72	12.54	10.00
CIFAR-100 dataset									
KAGN Simple 8 Layers V2	LSQ	68.06	67.20	65.87	68.49	68.41	52.36	53.01	47.00
	LSQ+		66.50	67.70	68.12	64.35	58.27	59.64	1.30
	DoReFa		67.93	66.89	53.58	23.39	29.49	9.66	8.62
	DSQ		67.12	68.03	67.54	43.10	34.01	35.45	43.10
	PACT		68.20	66.94	59.39	1.00	47.92	20.43	1.00
	QIL		68.11	61.14	1.02	1.00	2.19	1.01	1.00
VGG Like KAGN V2	LSQ	58.77	46.15	58.51	56.31	52.99	<b>1.00</b>	<b>1.00</b>	1.00
	LSQ+		58.05	56.98	<b>1.00</b>	30.18	<b>1.00</b>	<b>1.00</b>	1.01
	DoReFa		58.50	48.96	<b>1.00</b>	21.61	18.37	1.00	1.08
	DSQ		57.82	58.58	58.23	1.00	56.81	55.86	1.00
	PACT		58.64	30.97	25.09	1.00	7.13	1.16	1.00
	QIL		59.15	18.86	1.15	1.00	12.25	1.13	1.00

Table 11. Accuracy (%) of PTQ methods on different datasets under various bit-precision settings. (**w4** means **w4a32**, likewise **w3=w3a32**, **w2=w2a32**).

Architecture	Method	w32a32	w8	w4	w3	w2	w4a4	w3a3	w2a2
MNIST dataset									
KAN FCN	GPTQ		98.00	97.86	97.07	76.58	95.88	88.99	40.90
	Adaround		97.97	97.78	96.36	42.87	95.75	88.88	32.35
	AWQ		97.98	97.80	95.53	33.65	95.55	88.73	21.02
	BRECQ	97.99	73.77	72.58	73.60	50.51	70.87	86.93	52.38
	Uniform		97.97	97.81	96.15	39.48	97.81	96.15	39.48
	HAWQ-V2		97.97	97.97	97.81	96.14	—	—	—
	ZeroQ		98.00	97.75	96.86	48.89	95.19	90.81	29.06
KAN ConvNet	GPTQ		95.69	95.65	95.63	88.18	10.10	10.10	10.10
	Adaround		95.69	95.61	95.20	80.03	9.73	10.28	10.25
	AWQ		95.68	95.62	95.01	62.70	10.10	10.10	10.32
	BRECQ	95.69	36.37	37.79	30.31	35.07	75.60	93.52	64.97
	Uniform		95.68	95.51	94.51	68.63	95.51	94.51	68.63
	HAWQ-V2		95.68	95.69	95.49	94.37	—	—	—
	ZeroQ		95.70	95.67	95.52	84.32	10.10	10.10	8.92
KAGN Simple	GPTQ		98.65	97.96	90.11	27.39	97.96	90.11	27.39
	Adaround		98.76	96.59	88.41	29.83	96.59	88.41	29.83
	AWQ		98.70	97.35	57.65	13.36	97.35	57.65	13.36
	BRECQ	98.66	98.73	96.11	76.07	23.33	96.22	81.70	12.80
	Uniform		98.73	95.83	74.84	20.36	95.83	74.84	20.36
	HAWQ-V2		98.73	34.74	35.27	27.30	—	—	—
	ZeroQ		98.66	97.90	88.91	12.13	97.90	88.91	12.13
CIFAR-10 dataset									
KAGN Simple	GPTQ		62.36	56.52	40.85	11.68	56.52	40.85	11.68
	Adaround		62.27	53.92	34.21	11.61	53.92	34.21	11.61
	AWQ		62.17	54.01	22.01	9.58	54.01	22.01	9.58
	BRECQ	62.23	62.28	52.28	24.47	12.35	49.98	27.43	16.21
	Uniform		62.19	51.67	23.95	15.01	51.67	23.95	15.01
	HAWQ-V2		62.29	31.56	32.05	20.31	—	—	—
	ZeroQ		62.30	56.01	44.71	16.79	56.01	44.71	16.79
KAGN Simple 8 Layers	GPTQ		78.02	69.13	41.59	9.92	69.13	41.59	9.92
	Adaround		78.15	61.57	37.93	10.09	61.57	37.93	10.09
	AWQ		77.92	60.17	28.01	12.17	60.17	28.01	12.17
	BRECQ	78.08	77.88	60.28	27.64	12.82	62.28	39.31	19.20
	Uniform		77.91	59.47	30.17	9.11	59.47	30.17	9.11
	HAWQ-V2		77.89	43.13	28.29	24.29	—	—	—
	ZeroQ		77.94	70.41	39.71	13.31	70.41	39.71	13.31
CIFAR-100 dataset									
KAGN Simple 8 Layers V2	GPTQ		68.05	13.47	2.65	1.14	13.47	2.65	1.14
	Adaround		67.67	2.77	1.01	1.00	2.77	1.01	1.00
	AWQ		67.62	3.74	1.00	1.00	3.74	1.00	1.00
	BRECQ	68.09	67.57	3.86	1.00	1.00	3.12	1.49	1.47
	Uniform		67.66	3.74	1.00	1.00	3.74	1.00	1.00
	HAWQ-V2		67.57	1.62	1.08	1.03	—	—	—
	ZeroQ		68.07	13.06	2.24	1.46	13.06	2.24	1.46
VGG Like KAGN V2	GPTQ		58.23	39.73	14.23	1.98	39.57	13.26	0.99
	Adaround		55.91	22.66	6.05	1.47	22.63	5.46	1.03
	AWQ		58.30	29.57	13.44	1.22	29.44	12.48	1.15
	BRECQ	58.70	58.29	29.80	15.64	1.88	32.17	15.99	2.57
	Uniform		55.88	21.08	3.65	1.15	21.08	3.65	1.15
	HAWQ-V2		58.31	12.06	7.99	5.56	—	—	—
	ZeroQ		58.17	39.68	14.29	1.55	39.47	13.85	1.15

Table 12. Full ablation results on CIFAR10 with quantization applied to **weights**. Each cell reports Top-1 accuracy (%).

Variant	Bits	DoReFa				DSQ				LSQ			
		Asym-Ch	Asym-T	Sym-Ch	Sym-T	Asym-Ch	Asym-T	Sym-Ch	Sym-T	Asym-Ch	Asym-T	Sym-Ch	Sym-T
		49.67	49.60	49.78	49.77	49.87	49.93	49.82	49.41	49.78	49.84	49.78	49.75
eff kan	w8a32	49.34	49.74	49.34	49.59	49.39	49.61	49.53	49.65	49.64	49.76	49.73	49.69
	w4a32	49.56	48.67	49.36	49.31	49.71	49.63	49.67	49.57	49.39	49.51	49.26	49.17
	w3a32	47.87	48.04	48.12	48.62	49.92	49.66	49.54	49.33	49.78	48.65	48.57	48.22
	w4a4	44.72	44.67	44.75	44.68	49.72	50.16	49.63	49.76	32.68	33.65	33.08	33.86
	w3a3	44.43	44.30	44.25	44.42	49.87	50.02	49.84	49.88	33.80	33.26	33.19	33.39
	w2a2	41.81	42.10	42.04	41.87	49.85	49.97	50.42	50.17	32.75	32.70	32.52	32.25
	w8a32	39.93	39.86	39.74	40.26	39.97	39.76	40.11	39.94	39.70	41.57	40.12	39.76
fastkan	w4a32	39.28	39.01	39.38	39.13	39.75	40.47	40.17	40.18	39.40	39.35	39.75	39.11
	w3a32	37.17	37.33	37.41	37.86	40.21	40.14	40.06	40.37	38.27	40.40	39.56	40.91
	w2a32	30.97	31.07	31.16	30.42	40.22	40.95	40.40	40.93	40.32	41.44	40.07	41.44
	w4a4	30.12	29.99	29.58	29.84	35.58	10.00	35.69	36.57	28.34	28.01	27.24	28.21
	w3a3	28.07	28.34	29.06	29.26	35.86	10.00	34.48	35.73	27.15	31.50	27.42	31.22
	w2a2	24.81	25.15	24.84	25.24	34.76	10.00	34.55	10.00	25.03	30.52	28.88	30.73
	w8a32	49.89	49.79	49.71	49.85	49.76	49.44	49.52	49.68	46.57	47.92	48.49	49.68
gramlayer	w4a32	50.08	49.82	49.74	50.06	50.03	49.48	49.67	49.91	48.67	49.39	48.54	49.76
	w3a32	49.54	49.46	49.82	49.85	49.67	49.52	49.84	49.82	49.63	49.50	49.06	49.60
	w2a32	49.28	49.23	49.54	49.34	49.72	49.45	49.76	50.20	48.56	48.79	48.22	48.54
	w4a4	44.06	44.49	44.40	43.66	48.89	49.29	48.95	48.87	41.60	41.37	40.83	41.62
	w3a3	44.03	43.53	43.86	43.42	49.02	49.19	49.12	48.77	40.95	40.62	41.14	40.90
	w2a2	41.16	41.07	40.97	41.44	48.63	48.91	48.80	49.00	37.63	37.74	31.29	31.73
	w8a32	50.84	50.69	50.92	50.33	50.53	50.42	50.58	50.23	50.50	50.35	50.74	50.97
pykan	w4a32	50.62	50.51	50.27	50.57	50.47	50.78	50.41	50.88	50.21	50.41	50.97	50.15
	w3a32	50.01	50.27	50.51	49.98	50.76	50.98	50.75	50.65	50.24	50.26	50.32	50.51
	w2a32	49.16	49.79	49.66	49.61	50.21	50.69	50.38	50.60	50.41	49.59	49.98	49.05
	w4a4	44.82	44.84	45.14	44.89	50.72	50.76	50.67	50.77	31.76	31.96	31.63	32.48
	w3a3	44.49	44.38	44.52	44.46	51.02	50.53	51.10	51.28	32.16	31.88	31.75	32.26
	w2a2	41.85	42.01	41.76	41.78	51.16	50.96	51.05	50.87	31.54	31.85	30.85	31.32

 Table 13. Full ablation results on CIFAR10 with quantization applied to **activations**. Each cell reports Top-1 accuracy (%).

Variant	Bits	DoReFa				DSQ				LSQ			
		Asym-Ch	Asym-T	Sym-Ch	Sym-T	Asym-Ch	Asym-T	Sym-Ch	Sym-T	Asym-Ch	Asym-T	Sym-Ch	Sym-T
		49.56	49.86	49.60	49.74	49.75	49.65	49.56	49.62	49.47	49.38	49.65	49.76
eff kan	w8a32	49.33	49.69	49.75	49.51	49.69	49.46	49.55	49.78	49.83	49.45	49.54	49.53
	w3a32	49.15	48.98	49.24	49.30	49.78	49.90	49.75	49.63	49.26	48.90	49.52	49.44
	w2a32	48.32	48.06	47.91	48.63	49.44	49.79	49.56	49.61	48.80	49.08	48.36	48.80
	w4a4	44.54	44.71	44.55	44.76	49.75	49.60	49.74	49.84	33.51	32.95	33.85	33.31
	w3a3	44.55	44.52	44.78	44.35	49.94	49.94	49.74	49.99	34.62	33.06	34.18	33.19
	w2a2	42.19	41.88	41.64	41.92	49.75	50.16	49.94	50.17	32.92	32.43	33.20	32.38
	w8a32	39.90	39.97	39.95	40.08	40.33	39.85	40.08	39.71	39.38	39.48	38.87	39.20
fastkan	w4a32	39.35	39.36	39.08	39.40	40.16	40.05	40.23	40.03	38.19	39.30	39.52	39.06
	w3a32	37.53	37.37	37.90	37.78	40.04	39.87	39.84	40.17	38.66	39.22	38.48	39.15
	w2a32	31.12	30.83	31.31	31.18	39.96	40.11	40.01	40.09	40.80	40.22	40.82	40.27
	w4a4	30.78	29.67	30.22	30.10	37.31	36.16	36.22	36.83	28.39	28.23	28.49	28.20
	w3a3	28.51	28.29	28.50	28.75	36.12	36.60	36.22	35.96	29.35	27.97	28.71	27.24
	w2a2	25.25	25.13	25.10	25.12	32.38	34.95	33.29	33.62	30.20	29.06	27.75	26.65
	w8a32	50.04	49.46	49.65	49.71	50.04	49.56	49.56	50.19	50.12	49.65	47.85	48.47
gramlayer	w4a32	49.51	49.73	49.88	49.88	49.89	49.84	49.51	49.69	49.58	49.16	49.61	49.72
	w3a32	49.55	49.65	49.68	49.58	49.74	49.78	50.35	49.67	49.55	49.35	48.87	49.44
	w2a32	49.13	48.88	48.76	48.89	50.14	49.78	50.18	50.04	48.42	48.70	48.92	48.26
	w4a4	43.89	44.35	44.35	43.75	48.84	49.12	48.86	48.74	41.68	41.40	41.12	40.63
	w3a3	43.22	43.86	43.68	43.37	48.47	48.55	48.66	49.02	41.00	40.25	41.21	41.10
	w2a2	41.01	40.99	41.26	40.48	48.29	48.90	48.99	48.95	31.81	31.53	32.10	30.75
	w8a32	50.78	50.64	50.79	50.42	50.52	50.67	50.37	50.43	50.55	50.56	50.69	
pykan	w4a32	50.57	50.44	50.44	50.45	50.61	50.34	50.53	50.52	50.15	50.65	50.39	50.41
	w3a32	50.43	50.34	50.30	50.20	50.71	50.54	50.91	50.34	49.96	50.08	49.85	49.77
	w2a32	50.64	49.50	49.13	50.28	50.47	50.41	50.53	50.57	50.17	49.87	49.71	50.29
	w4a4	44.90	44.64	44.77	44.82	50.68	50.87	50.69	50.66	32.06	32.13	32.73	31.93
	w3a3	44.37	44.68	44.72	44.32	50.68	51.01	50.78	50.61	33.06	31.70	33.25	31.86
	w2a2	42.16	41.61	41.77	41.68	50.74	50.84	51.09	50.69	33.20	31.34	32.80	31.75

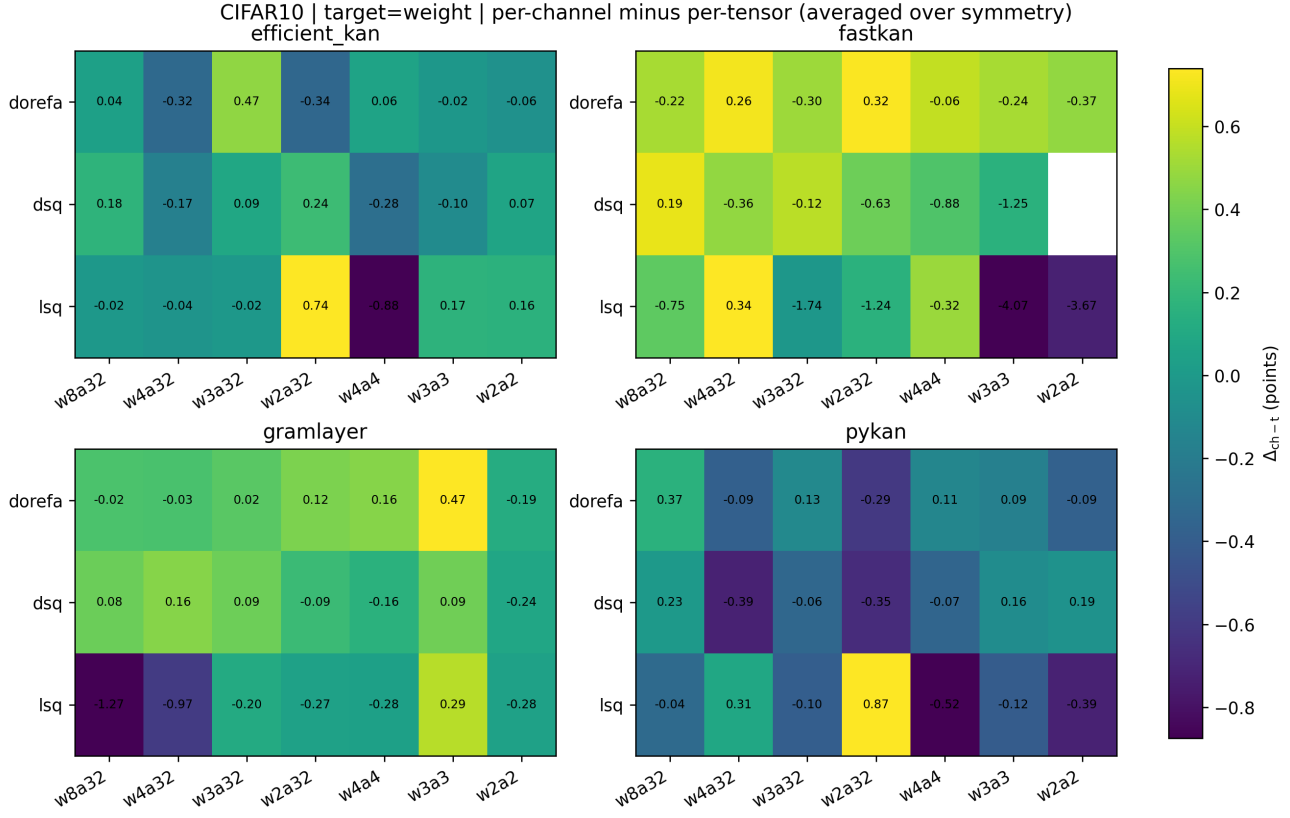


Figure 10. Granularity sensitivity for **weight** quantization on CIFAR-10. Each panel corresponds to a KAN variant; cells report  $\Delta_{ch-t}$  (per-channel minus per-tensor accuracy, averaged over symmetric/asymmetric ranges) across quantizers and bit-widths.

Table 14. Full parameter-wise sensitivity under single-parameter mixed precision. We report mean degradation  $\Delta = \max(0, \text{Acc}_{FP} - \text{Acc})$  when quantizing a single parameter group to bit-width  $b \in \{2, 3, 4\}$  while keeping all others at 8-bit (lower is better).

Variant	Parameter	CIFAR-10			MNIST		
		$b=2$	$b=3$	$b=4$	$b=2$	$b=3$	$b=4$
EFF-DSQ	$w_{base}$	0.00	0.00	0.00	0.00	0.00	0.00
	$w_{scaler}$	0.00	0.00	0.00	0.00	0.00	0.00
	$w_{spline}$	0.00	0.00	0.00	0.00	0.00	0.00
EFF-LSQ	$w_{base}$	0.43	0.00	0.00	<b>0.74</b>	0.06	0.00
	$w_{scaler}$	0.00	0.00	0.00	0.00	0.00	0.00
	$w_{spline}$	0.00	0.00	0.00	0.00	0.00	0.00
FAST-DSQ	$w_{base}$	0.00	0.00	0.00	0.00	0.00	0.00
	$w_{spline}$	0.00	0.00	0.00	0.00	0.00	0.00
FAST-LSQ	$w_{base}$	0.00	0.00	0.00	<b>0.14</b>	0.00	0.00
	$w_{spline}$	<b>3.07</b>	1.05	0.00	0.00	0.00	0.00
GRAM-DSQ	$w_{base}$	0.00	0.14	0.36	0.00	0.00	0.00
	$w_{beta}$	0.00	0.07	0.12	0.00	0.00	0.00
	$w_{gram}$	0.00	0.00	0.05	0.00	0.00	0.00
GRAM-LSQ	$w_{base}$	<b>2.92</b>	0.04	0.00	0.31	0.06	<b>0.48</b>
	$w_{beta}$	0.00	0.00	0.00	0.00	0.00	0.00
	$w_{gram}$	<b>2.62</b>	0.33	2.46	<b>0.46</b>	0.00	0.11
PyKAN-DSQ	$w_{coef}$	0.00	0.00	0.00	0.00	0.00	0.00
	$w_{scale,base}$	0.00	0.00	0.00	0.00	0.00	0.00
	$w_{scale,sp}$	0.00	0.00	0.00	0.00	0.00	0.00
PyKAN-LSQ	$w_{coef}$	—	0.00	0.00	0.00	0.00	0.00
	$w_{scale,base}$	<b>0.66</b>	—	0.00	<b>0.30</b>	0.02	0.00
	$w_{scale,sp}$	0.00	0.00	0.00	0.00	0.00	0.00

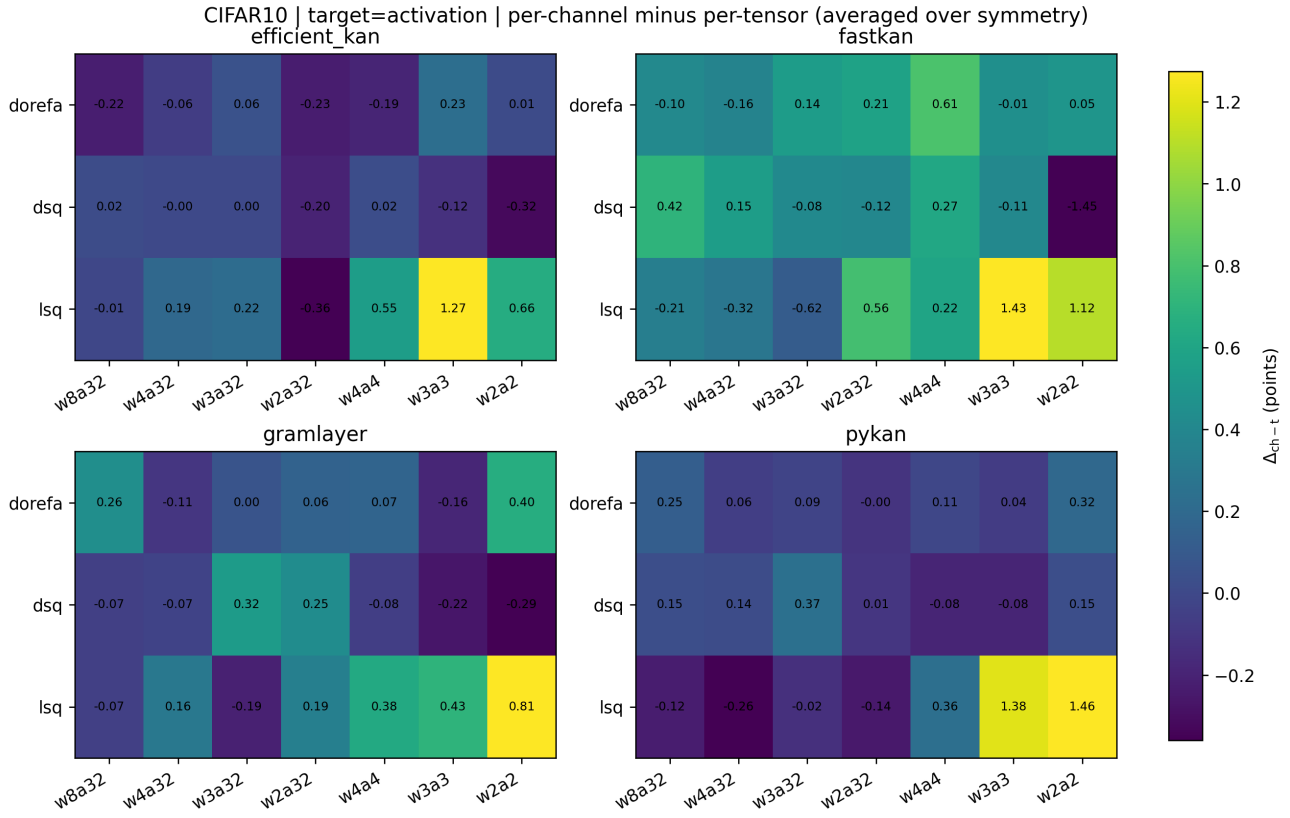


Figure 11. Granularity sensitivity for **activation** quantization on CIFAR-10. Each panel corresponds to a KAN variant; cells report  $\Delta_{ch-t}$  (per-channel minus per-tensor accuracy, averaged over symmetric/asymmetric ranges) across quantizers and bit-widths.